TEKTONIKA

Setting the Sequence of Slicing Events Along Deep Subduction Interfaces: 1. The Tectonic and Thermal Structure of the High-*P* Duplex in Western Crete (Hellenic Margin)

Armel Menant *[1,2], **Romain Augier** [3], **Eloïse Bessière** [1], **Samuel Angiboust** [4,5], **Laurent Jolivet** [6], **Onno Oncken** [2]

[1]Université Côte d'Azur, CNRS, Observatoire de la Côte d'Azur, IRD, Géoazur, Valbonne, France | [2]GFZ Helmholtz Centre Potsdam, German Research Centre for Geosciences, Potsdam, Germany | [3]Université d'Orléans, Institut des Sciences de la Terre d'Orléans (ISTO), CNRS, BRGM, UMR7327, Orléans, France | [4]École Normale Supérieure of Lyon, Université de Lyon, LGL-TPE, Lyon, France | [5]Institut Universitaire de France (IUF), Paris, France | [6]Sorbonne Université, CNRS-INSU, Institut des Sciences de la Terre de Paris (ISTeP), UMR7193, Paris, France

Abstract Basal accretion at active subduction margins occurs through a series of tectonic slicing events at varying depths along the plate interface, shaping the forearc domain. To assess the spatial and temporal scale of the accretion-controlled forearc dynamics, it is crucial to constrain the sequence of basal-accretion episodes that form deep accretionary duplexes. This requires identifying the successive tectono-metamorphic units constituting paleo-duplexes and dating the accretion and exhumation events that expose high-pressure rocks at the surface. This, the first of two companion papers in this issue of Tektonika, presents a detailed reconstruction of the tectonic and thermal structure of a high-pressure/low-temperature paleo-accretionary duplex in western Crete (Greece) that formed along the active Hellenic margin during the Oligocene-Miocene. Combining field observations, structural measurements and Raman spectroscopy on carbonaceous material (RSCM), we identify five tectono-metamorphic slices (i) bounded by shear zones often reworked during exhumation and (ii) characterized by a down-stepping of peak metamorphic temperatures towards lower structural levels. Our geological and structural mapping reveals the overall geometry of the nappe stack forming a dome-like structure, exhumed beneath major top-to-the-N and subordinate top-to-the-S detachments that accommodated N-S-directed crustal extension. This trench-perpendicular extension was intermittently rotated into an E-W direction (trench-parallel), as evidenced by a newly recognized top-to-the-W ductile-brittle detachment. Minor compressional events did not significantly alter the 3D architecture of the paleo-duplex. Reported RSCM peak metamorphic temperatures of ~350-450 °C from the nappe stack align with the typical temperature range for the downdip limit of the seismogenic zones, suggesting a first-order thermo-mechanical control on the depth of basal accretion along the subduction interface. These findings provide crucial constraints for interpreting the deep-accretion and exhumation dynamics that shaped the long-term evolution of the Hellenic forearc domain.

Executive Editor:
Graeme Eagles
Associate Editor:
Laura Federico
Technical Editor:
Mohamed Gouiza

Reviewers:
Edoardo Sanità
Reviewer 2
(Anonymous)

Submitted:
31 March 2025
Accepted:
30 December 2025
Published:
9 April 2026

1 Introduction

Mass flux through the subduction interface plays a significant control in forearc formation and destruction (*von Huene and Scholl*, 1991; *Lallemand et al.*, 1994; *Noda*, 2016), crustal growth (*Clift and Vannucchi*, 2004) and the frictional properties and seismic behavior of the megathrust (*Wang and Hu*, 2006; *Bassett and Watts*, 2015; *Scholl et al.*, 2015). Building on the pioneering subduction-channel model by *Cloos and Shreve* (1988), accretion and tectonic erosion are commonly described, either explicitly or implicitly, as steady-state flow over Myr timescales (*Ring et al.*, 1999; *Burov et al.*, 2001; *Schwartz et al.*, 2001; *Gerya et al.*, 2002; *Erdman and Lee*, 2014). However, this simple yet practical framework is increasingly challenged by geological and geophysical evidence pointing to the transient nature of these mass transfers in space and time. Tectonic segmentation of present-day forearc domains is thus influenced by both along-strike and along-dip variations in accretionary and erosive processes (*Clift and Hartley*, 2007; *Polonia et al.*, 2007; *Sutherland et al.*, 2009). Additionally, Myr-scale temporal variations have been reported,

*✉ armel.menant@geoazur.unice.fr

controlled by varying trench sediment supply and, more broadly, by significant changes in the hydro-mechanical properties of the plate interface (*Bangs and Cande*, 1997; *Kopp*, 2013; *Angiboust et al.*, 2022). Analog and numerical models also predicted that long-lasting accretion periods are characterized by a sequential growth of a wedge driven by the succession of frontal and/or basal accretion events (*Gutscher et al.*, 1996; *Lohrmann et al.*, 2006; *Hoth et al.*, 2007; *Menant et al.*, 2020; *Ruh*, 2020). The recognition of coherent tectonic slices constituting most of the now-exhumed accretionary complexes studied worldwide (also called "duplex") (*Platt*, 1986; *Maruyama et al.*, 1996; *Guillot et al.*, 2009; *Agard et al.*, 2018; *Angiboust et al.*, 2018) support these model predictions. It also highlights the existence of a usually overlooked accretion-driven tectonic and topographic signal along subduction zones where ongoing accretion events are proven or suspected (*Scholl*, 2019). Appraising the sequence of tectonic slicing and therefore the characteristic wavelength of its crustal signature is, therefore, a critical goal to achieve because it plays a part in active forearc deformations monitored at convergent margins worldwide.

Evaluating the time frame of distinct accretion events occurring at 20-50 km depth is challenging, though it has major implications on the geological and tectonic environment of deep-seated episodic tremor and slow slip events (ETS) along the plate interface (*Angiboust et al.*, 2015; *Bassett and Watts*, 2015; *Behr and Bürgmann*, 2021). Combined field and geochronological investigations have, nonetheless, unraveled consistent decreasing age patterns for the high-pressure-low temperature (HP-LT) metamorphism, from the top to the base of several paleo-duplexes, providing maximum bounds for deep-slicing recurrence ranging between ~1-2 Myr and ~6-8 Myr (*Agard et al.*, 2002; *Bachmann et al.*, 2009; *Dumitru et al.*, 2010; *Vitale Brovarone and Herwartz*, 2013; *Angiboust et al.*, 2014; *Glodny and Ring*, 2022; *Uunk et al.*, 2022). The apparent spreading of the recurrence time for basal accretion events strongly depends on (i) the difficulty to identify successive tectono-metamorphic units, (ii) the lack of preservation of some of these units and (iii) the accuracy of geochronological data. A way to tackle this issue would consist in focusing efforts on young paleo-duplexes cropping out in their initial forearc position because of the limited superimposition of post-subduction metamorphic and structural imprint and the decreasing uncertainty on age determinations.

In the present two companion papers, we report a multi-disciplinary study to unravel with an unprecedented resolution the tectono-metamorphic evolution of the paleo-accretionary complex exposed in western Crete, Greece (Figure 1) (*Creutzburg and Seidel*, 1975; *Papanikolaou and Vassilakis*, 2010). These rocks are part of the Oligocene-Miocene HP-LT belt exhumed in a syn-orogenic context in the forearc domain of the active Hellenic subduction zone (*Seidel et al.*, 1982; *Fassoulas et al.*, 1994; *Jolivet et al.*, 1994, 1996; *Wicker and Bufféral*, 2024; *Bouhot et al.*, 2025), making this region exemplary for investigating the sequence of past (though recent) basal-accretion events occurring at active convergent margins. The tectonic evolution of the metamorphic complex in Crete is intensively debated, with opposing models involving an early nappe stacking followed by an exhumation stage mainly achieved under either dominant extension (*Fassoulas et al.*, 1994; *Jolivet et al.*, 1996, 2010; *Papanikolaou and Vassilakis*, 2010; *Grasemann et al.*, 2019), continuous compression (*Chatzaras et al.*, 2013; *Ring and Yngwe*, 2018) or a complex sequence of compressional and extensional episodes (*Zulauf et al.*, 2002).

This first contribution provides new field observations, structural measurements and Raman spectrometry on carbonaceous material (RSCM) analyses to constrain the 3D geometry and thermal architecture of the paleo-duplex of western Crete. Five tectono-metamorphic units are identified and interpreted as successive basal-accretion events. They are all characterized by distinct peak metamorphic temperatures and bounded by major shear zones that commonly exhibit a partial reworking during exhumation. The subsequent unroofing of the HP-LT rocks has, then, been achieved below two low-angle normal fault zones (i.e., detachments) accommodating a N-S-directed, bivergent extension later evolving to an E-W-directed, trench-parallel extension, contributing to the final geometry of the paleo-duplex as a dome-like structure. These outcomes will be used in the second contribution (*Menant et al.*, 2026, this issue), together with new petrological observations, P-T pseudosection modeling, Rb/Sr multi-mineral geochronology and U-Th/He thermochronology on zircon, to reconstruct the P-T-t evolution of the previously identified tectono-metamorphic units and to provide new insights into the long-term basal-accretion dynamics of the Hellenic subduction zone.

2 Geological Setting

2.1 Geodynamic Overview of the Hellenic Subduction Zone

The active Hellenic margin results from the northward subduction of oceanic and continental domains, driven by the convergence of Africa and Eurasia since the Mesozoic (*Pichon and Angelier*, 1979; *Dercourt et al.*, 1986; *Menant et al.*, 2016; *Romagny et al.*, 2020; *van Hinsbergen et al.*, 2020). Over time, the upper crustal section of these domains successively accreted to the Eurasian margin, forming the Hellenides, a nappe stack composed of low-grade metamorphic units (*Aubouin*, 1959; *Papanikolaou*, 1997; *van Hinsbergen et al.*, 2005a). Acceleration of southward slab rollback in the Oligocene-Miocene triggered the collapse of the Hellenides and the opening of the Aegean back-arc domain, leading to the exhumation of deep crustal sections as Cordilleran-type metamorphic core complexes (*Lister et al.*, 1984; *Gautier et al.*, 1993; *Jolivet and Brun*, 2010; *Ring et al.*, 2010; *Beaudoin et al.*, 2015). In the Cyclades, these rocks form the Cycladic Blueschist Unit that is directly exposed below the low-grade metamorphic units and preserves

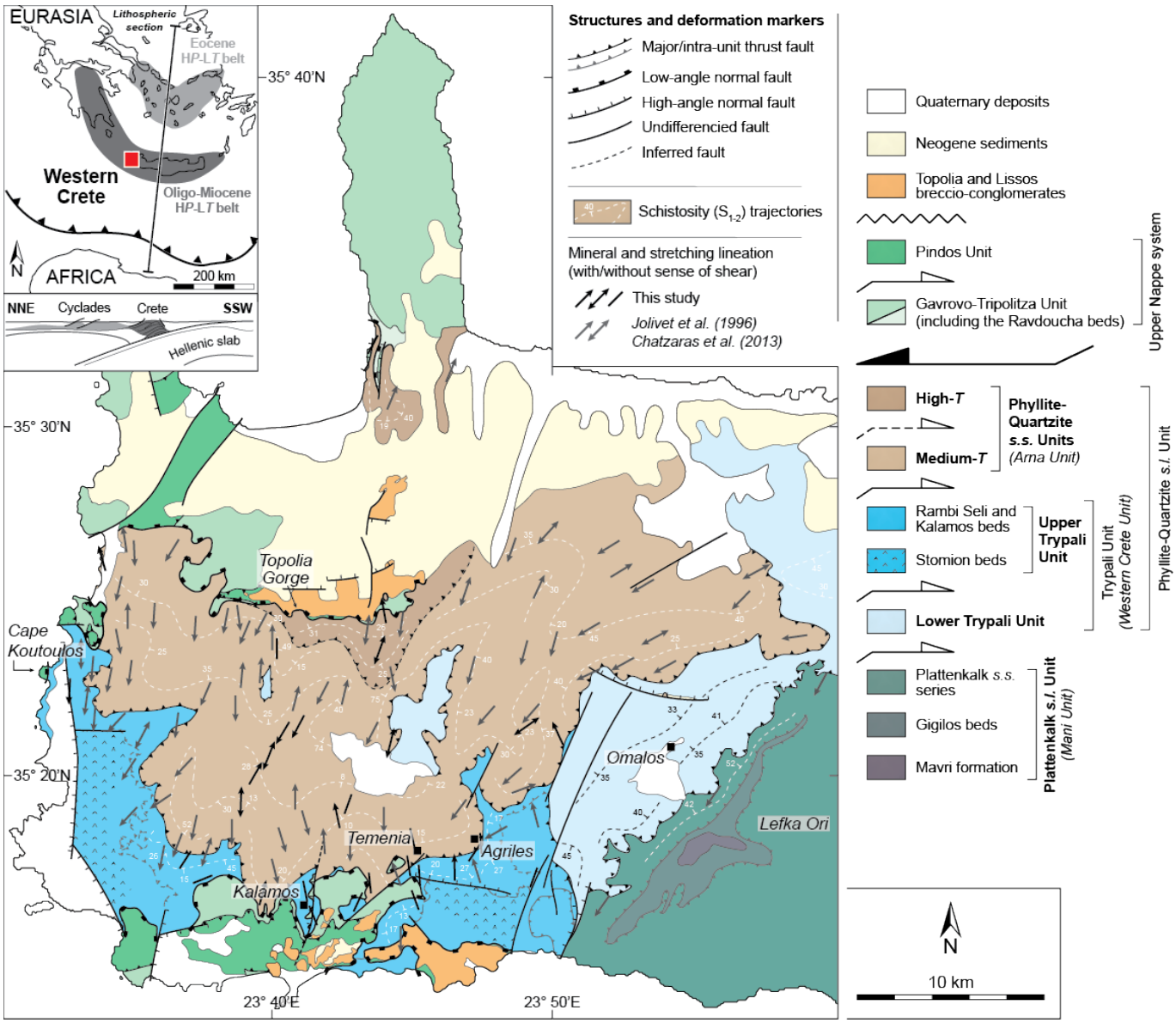

Figure 1 – Geological and structural map of western Crete compiled from *Creutzburg and Seidel* (1975); *Seidel et al.* (2007); *Chatzaras et al.* (2013); *Zulauf et al.* (2018) and this study. Schistosity trajectories are derived from measurements by *Chatzaras et al.* (2013) and this study. The inset map and lithospheric-scale cross-section show the location of the study area (modified from *Menant et al.* (2016). Arrowheads on mineral and stretching lineation markers indicate sense of shear.

a subduction-related H*P*-L*T* imprint from the early Eocene (*Bonneau and Kienast*, 1982; *Wijbrans and McDougall*, 1986; *Jolivet*, 2003; *Laurent et al.*, 2021). The Cycladic Blueschist Unit distinguishes up to four main sub-units, each defined by distinct metamorphic stages that are interpreted as successive accretion events at the base of the Hellenic wedge during the Eocene-Oligocene (*Grasemann et al.*, 2018; *Roche et al.*, 2019; *Glodny and Ring*, 2022; *Kotowski et al.*, 2022; *Uunk et al.*, 2022). Additional subunit divisions have been proposed for the Cycladic Blueschist Unit (*Laurent et al.*, 2016), suggesting that some basal-accretion events may have been overlooked.

As the Aegean back-arc opened, the Hellenic subduction zone continued to migrate south, leading to the formation and exhumation of an Oligocene-Miocene H*P*-L*T* belt from Crete to Peloponnese (*Seidel et al.*, 1982; *Jolivet et al.*, 1996, 2010; *Thomson et al.*, 1998; *van Hinsbergen et al.*, 2005b; *Marsellos et al.*, 2010). Western Crete lies in the central part of this belt (see inset of Figure 1) above the current plate interface where active basal accretion is inferred, suggesting a protracted basal-accretion history along this segment of the Hellenic margin (*Angelier et al.*, 1982; *Jolivet et al.*, 1994; *Gallen et al.*, 2014; *Ott et al.*, 2019).

2.2 The Nappe Stack in Western Crete

In Crete, most nappes described in the Hellenides are present, including units with subduction-related H*P*-L*T* metamorphism (*Aubouin*, 1959; *Seidel et al.*, 1982; *Bonneau*, 1984; *Papanikolaou*, 1997). Below, we review the succession of tectono-metamorphic and tectono-stratigraphic units exposed in western Crete (Figure 1).

The H*P*-L*T* complex is typically divided into two tectono-metamorphic units: the Phyllite-Quartzite *sensu lato* (*s.l.*) Unit and the Plattenkalk *s.l.* Unit that subducted beneath Eurasia during the Oligocene-middle Miocene (*Bonneau*, 1984; *Jolivet et al.*, 1996; *van Hinsbergen et al.*, 2005a). Structurally below, the Plattenkalk *s.l.* Unit, also referred as the Mani Unit (*Papanikolaou and Vassilakis*, 2010), forms a ~5 km-thick sedimentary sequence ranging from Permian to early Oligocene. In western Crete, its upper portion is well-exposed in the Lefka Ori massif and includes, from base to top, stromatolite-rich dolomites (the Mavri formation), siliciclastic layers with interbedded phyllites, calcschists, cherts and carbonates (the Gigilos beds) and platy marbles with chert nodules (the Plattenkalk *sensu stricto* (*s.s.*) series) (Figures 1, 2) (*Soujon et al.*, 1998; *Fassoulas et al.*, 2004). The uppermost section of the Plattenkalk *s.l.* Unit locally exposes calcschist layers (the Kalavros formation), more developed in central and eastern Crete (*Soujon et al.*, 1998).

The recognition of *Mg*-carpholite and coexisting pyrophyllite and diaspore in rare metabauxite horizons within the Plattenkalk *s.l.* Unit suggest metamorphic conditions of >7 kbar and 350-400 °C (*Seidel et al.*, 1982). Independent temperature estimates from RSCM thermometry indicate peak metamorphic temperatures of ~340 °C for this unit in central and western Crete, with a significant scatter between 275 °C and 443 °C (*Rahl et al.*, 2005).

Several subdivisions have been proposed for the Phyllite-Quartzite *s.l.* Unit that tectonically overlays the Plattenkalk *s.l.* Unit. The succession described below is based on a compilation of lithostratigraphic, structural and radiochronologic evidences alongside new field observations and RSCM results presented in this study (Figures 1, 2) (*Creutzburg and Seidel*, 1975; *Krahl et al.*, 1983; *Wernado*, 1983; *Zulauf et al.*, 2018). The lowermost Trypali Unit, also called the Western Crete Unit (*Papanikolaou and Vassilakis*, 2010), comprises early Triassic-early Jurassic metasediments with increasing depositional age upwards, suggesting either an overturned stratigraphy (*Krahl et al.*, 1983; *Zulauf et al.*, 2018) or a stacked nappe sequence (*Chatzaras et al.*, 2013). Its base is well exposed at Omalos and consists of ~800 m-thick massive marbles with locally brecciated facies. Above lie gypsum layers with metamorphic graywackes and slightly bituminous dolomites (the Stomion beds), followed by alternating marbles and phyllites (the Kalamos beds, ~300 m thick). These are in turn overlain by intercalated marbles, phyllites, quartzites, metaconglomerates and metavolcanics (the Rambi Seli beds, ~400 m thick). The Trypali Unit is overlain by the Phyllite-Quartzite *s.s.* Unit, also called the Arna Unit (*Papanikolaou and Vassilakis*, 2010), with intercalated quartzites and phyllites and minor marbles, metaconglomerates and metavolcanics with depositional ages ranging from late Carboniferous to late Triassic-early Jurassic (*Krahl et al.*, 1983; *Zulauf et al.*, 2018). The contact between the Trypali Unit and the Phyllite-Quartzite *s.l.* Unit is commonly described as a thrust, known as the Phyllite-Quartzite (or Arna) basal thrust (Figure 1) (*Papanikolaou and Vassilakis*, 2010; *Chatzaras et al.*, 2013), whereas the other contacts are often envisioned as facies transitions (*Krahl et al.*, 1983; *Zulauf et al.*, 2018). A notable exception is the ductile Kalamos thrust at the base of the Kalamos beds (*Chatzaras et al.*, 2013). More recently, *Ring et al.* (2022) proposed an alternative sub-division for the Phyllite-Quartzite *s.l.* Unit into, the upper and lower Phyllite-Quartzite Units, along a ~E-W-trending fault zone marked with top-to-the-S kinematic indicators.

The Phyllite-Quartzite *s.l.* Unit preserves a blueschist-facies metamorphism, with peak metamorphic conditions of 10 ± 3 kbar and 400 ± 50 °C (*Seidel et al.*, 1982; *Theye et al.*, 1992; *Vidal et al.*, 1992), although *Jolivet et al.* (1996) reported pressures as high as 16-18 kbar in western Cete. Despite a significant scatter between 260 °C and 448 °C, RSCM data partly overlap with these temperatures (*Rahl et al.*, 2005). K/Ar and $^{40}Ar/^{39}Ar$ dating on white micas indicate that the H*P*-L*T* event occurred ~20-25 Myr ago (*Seidel et al.*, 1982; *Jolivet et al.*, 1996), while U/Pb dating of aragonite-bearing veins yields younger ages of ~13-16 Ma (*Ring et al.*, 2022), pointing to a protracted metamorphic event.

The H*P*-L*T* complex is tectonically overlain by the Upper Nappe system that shows no or low-*P* metamorphism related to the Hellenic subduction event (*Wernado*, 1983; *Papanikolaou*, 1997; *Papanikolaou and Vassilakis*, 2010). The lowermost Gavrovo-Tripolitza Unit consists of Triassic volcano-sedimentary deposits, the Ravdoucha beds (equivalent to the Tyros beds exposed in Peloponnese), passing to a thick carbonate platform of Triassic-Eocene age and a late Eocene-Oligocene flysch. Above lies the Pindos Unit comprising late Triassic to Paleocene pelagic limestones and radiolarites covered by an Eocene-Oligocene flysch. The whole nappe stack is partly overlain by sedimentary basins containing early to middle Miocene coarse conglomerates interpreted as alluvial fan deposits (the Topolia and Lissos formations), followed by a late Miocene to early Pliocene succession of shallow marine limestones and marls (*van Hinsbergen and Meulenkamp*, 2006; *Seidel et al.*, 2007; *Zachariasse and van Hinsbergen*, 2025).

The tectonic contact between the H*P*-L*T* complex and the Upper Nappe system marks a minimum pressure gap of ~10 kbar, implying a >30 km thickness of missing crust (*Jolivet et al.*, 2010). However, its nature and its polyphased character remain debated. It is, thus, described as a ductile-brittle detachment zone with top-to-the-N kinematics (*Jolivet et al.*, 1994, 1996; *Ring et al.*, 2001; *van Hinsbergen et al.*, 2005b; *Grasemann et al.*, 2019) or as conjugated top-to-the-N and top-to-the-S detachments (*Fassoulas et al.*, 1994; *Papanikolaou and Vassilakis*, 2010) or as a top-to-the-S/-SSW out-of-sequence thrust (*Chatzaras et al.*, 2006, 2013; *Ring and Yngwe*, 2018). These contrasting interpretations lead to conflicting tectonic

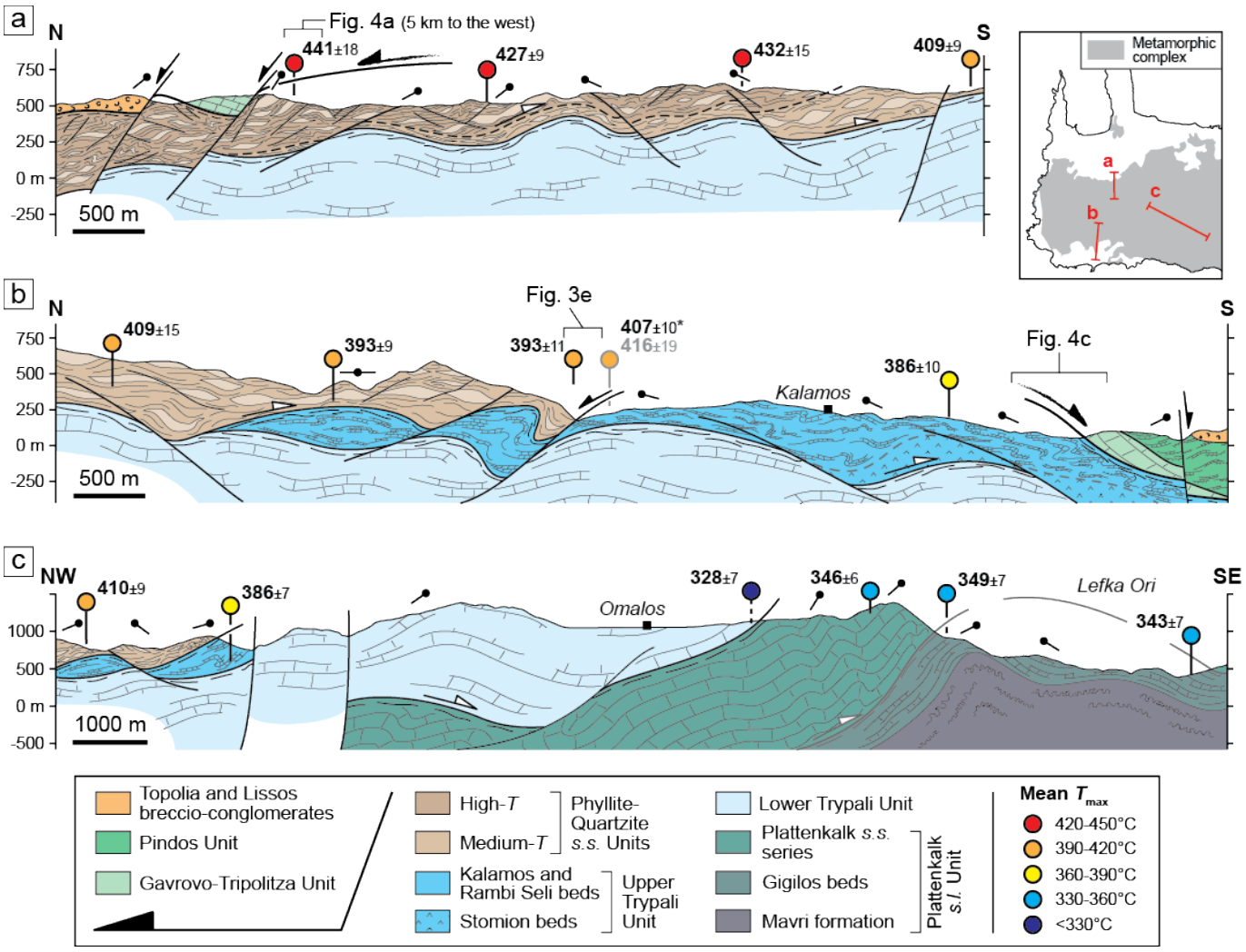

Figure 2 – Km-scale cross-sections illustrating the succession of tectono-metamorphic units and their relationship with the overriding Upper Nappe system. The three cross-sections (localized in the inset map) characterize the 2D geometry of the northern (**a**) and southern (**b**) flanks of the H*P*-L*T* complex, as well as the lowermost section of the nappe stack (**c**). Key outcrops from this study are shown, along with mean peak metamorphic temperatures (mean T_{max}) from RSCM analyses (see Section 5).

models for the exhumation of the metamorphic nappe stack that we review in the following section.

2.3 Structural Record and Exhumation Models in Western Crete

The earliest structural fabric in the metamorphic complex in western Crete consists of a penetrative schistosity (S_1), a N-S-trending stretching lineation (L_1) associated with H*P* minerals (e.g., glaucophane) and ENE-WSW-striking carpholite-bearing tension gashes (*Greiling*, 1982; *Fassoulas et al.*, 1994; *Jolivet et al.*, 1996; *Zulauf et al.*, 2002). Early south-verging isoclinal recumbent folds (F_1) with fold axes that tend to align with L_1, suggesting intense N-S stretching at peak metamorphic conditions, are related to deep accretion and/or early exhumation.

There is a continuum of deformation during exhumation, characterized by (i) a schistosity (S_2) subparallel to or crosscutting S_1, forming typical crenulation cleavage and (ii) a N-S- to NE-SW-trending stretching lineation (L_2) defined by stretched quartz, calcite and greenschist-facies minerals including white mica, chlorite and epidote (*Jolivet et al.*, 1994, 1996; *Stöckhert et al.*, 1999; *Chatzaras et al.*, 2013). Concomitant large-scale boudinage and opposing top-to-the-N and top-to-the-S shear indicators point to significant vertical thinning of the nappe stack during exhumation from blueschist- to greenschist-facies conditions (*Greiling*, 1982; *Fassoulas et al.*, 1994; *Jolivet et al.*, 1994, 1996; *Stöckhert et al.*, 1999; *Zulauf et al.*, 2002; *Marsellos et al.*, 2010; *Chatzaras et al.*, 2013). A second generation of S-vergent kink folds and open folds (F_2), with E-W to NE-SW axis, is also reported and has been interpreted either as the result of transient N-S compressional events during an extension-dominated exhumation stage (*Fassoulas et al.*, 1994; *Zulauf et al.*, 2002) or as evidence for a protracted compressional regime (*Chatzaras et al.*, 2013; *Ring and Yngwe*, 2018). Despite these differing interpretations, all structural evidence points to a dominant N-S direction of tectonic transport that prevailed throughout the early-middle Miocene exhumation of the metamorphic complex in Crete.

In the middle-late Miocene, E-W extension became prominent as suggested by a ~E-W-trending lineation observed locally in the metamorphic stack of western Crete (*Marsellos et al.*, 2010), as well as by the segmentation of sedimentary basins by large-scale E-W- and N-S-trending normal faults (*Zachariasse et al.*, 2011). This trench-parallel extension is interpreted as a consequence of the bending and fast southward retreat of the subduction zone following the tearing of the slab in the middle Miocene (*Marsellos et al.*, 2010; *Menant et al.*, 2016). Finally, Crete experienced significant uplift during the Pliocene-Quaternary, accompanied by left-lateral transpressional faulting (*van Hinsbergen and Meulenkamp*, 2006; *Chatzaras et al.*, 2013) and followed by the action of WNW-ESE- and NNE-SSW-striking high-angle normal faults that control the present-day topography and the coastline shape (Figure 1) (*Angelier et al.*, 1982; *Armijo et al.*, 1992; *Gallen et al.*, 2014; *Nicol et al.*, 2020).

In summary, while early compressional deformation related to deep nappe stacking is widely accepted, the stress regime prevailing during the subsequent exhumation of the metamorphic complex in Crete remains debated. Several models have been proposed: (i) dominant N-S then E-W extension (*Jolivet et al.*, 1994, 1996; *Marsellos et al.*, 2010; *Papanikolaou and Vassilakis*, 2010), (ii) protracted N-S compression and left-lateral transtension (*Chatzaras et al.*, 2013; *Ring and Yngwe*, 2018) or (iii) transient periods of compression and extension (*Fassoulas et al.*, 1994; *Zulauf et al.*, 2002). To address this debate, a detailed reassessment of the structural record and tectonic contacts, particularly the major ductile-brittle shear zones at the top of the H*P*-L*T* nappe stack, was conducted in this study.

3 RSCM Methodology

In this work, peak metamorphic temperatures (T_{max}) were quantitatively estimated using RSCM thermometry (*Beyssac et al.*, 2002; *Lahfid et al.*, 2010) to characterize the thermal structure of the H*P*-L*T* duplex in western Crete that is mostly composed of metasediments. These rocks often contain carbonaceous material derived from organic matter originally present in the protolith that undergoes carbonization and graphitization during diagenesis and metamorphism. These processes lead to chemical and structural transformations, from poorly organized carbonaceous material to graphite (*Wopenka and Pasteris*, 1993). Because graphitization is irreversible, the structure of carbonaceous material is useful for determining T_{max} even in strongly retrogressed rocks (*Augier et al.*, 2005; *Gabalda et al.*, 2009; *Beaudoin et al.*, 2015). Laser Raman microspectroscopy is used to characterize the degree of organization of carbonaceous material and so to quantify T_{max} using different calibration methods (*Beyssac et al.*, 2002; *Rahl et al.*, 2005; *Aoya et al.*, 2010; *Kouketsu et al.*, 2014). In this study, both the *Beyssac et al.* (2002) and *Lahfid et al.* (2010) calibrations were applied to cover the ~200-650 °C temperature range. The absolute T_{max} accuracy is ±50°C for *Beyssac et al.* (2002) and ±25 °C for *Lahfid et al.* (2010), with relative uncertainties as small as ~10-15 °C allowing detection of subtle temperature variations at the scale of the study area (*Beyssac et al.*, 2004; *Beaudoin et al.*, 2015).

Carbonaceous material-rich metasediments consisting of dark phyllites, marbles and shales were collected from the H*P*-L*T* units and the poorly-metamorphosed Ravdoucha beds. Raman spectra of carbonaceous material were obtained from polished thin sections of 44 samples using a Renishaw inVia Reflex microspectroscope (BRGM-ISTO, Orléans, France) with an argon laser source of 514.5 nm wavelength. The laser power was set to ~20 mW, with ~1 mW reaching the sample surface where the beam was focused using a Leica DM2500 microscope with a x100 objective (numerical aperture = 0.90). Following *Beyssac et al.* (2002), all analyses were performed beneath a transparent crystal (mainly quartz, calcite, dolomite or chloritoid) to avoid polishing defects on carbonaceous material. For each sample, 18 to 40 spectra were acquired with ~30 accumulations of 4-s acquisition periods in the extended scanning mode (700–2000 cm^{-1}) to capture the inner structural heterogeneity of carbonaceous material. All spectra were then processed using *PeakFit* software (Systat Software Inc.).

4 Field Constraints on the Architecture of the H*P*-L*T* Duplex

In this section, we present a compilation of field observations and structural measurements, as well as a description of key microstructures, which allowed us to refine the geological map of western Crete (Figure 1) and to provide a series of detailed cross-sections (Figure 2) illustrating the geometry of the H*P*-L*T* nappe stack.

4.1 Major Tectonic Contacts

In the field, pristine kinematics along major contacts, initially functioning as thrusts between the tectono-metamorphic units, are often overprinted by later tectonic reworking. One exception is the contact between the Upper Trypali Unit and the Medium-*T* Phyllite-Quartzite Unit (i.e., a subdivision of the Phyllite-Quartzite *s.s.* Unit defined by thermal arguments, see Section 5) exposed near the village of Temenia (i.e., corresponding to the Trypali thrust of *Chatzaras et al.*, 2013, Figures 1, 3a-b). Its footwall consists of a few-meter-thick mylonitic to ultramylonitic zone with intense grain-size reduction (i.e., <50 μm; Figure 3c) affecting impure marbles in the uppermost part of the Kalamos beds (belonging to the Upper Trypali Unit). The mylonitic foliation is well marked by an alternation of white-colored and dark-gray calcitic layers and very thin white-mica-rich layers dipping moderately towards the NE. Centimeter-sized rounded clasts of calcite are also observed, as well as a partly dismembered calcite vein with local asymmetric folding indicating apparent top-to-the-SW kinematics (Figure 3c). Boudins of dolomite-rich layers with an

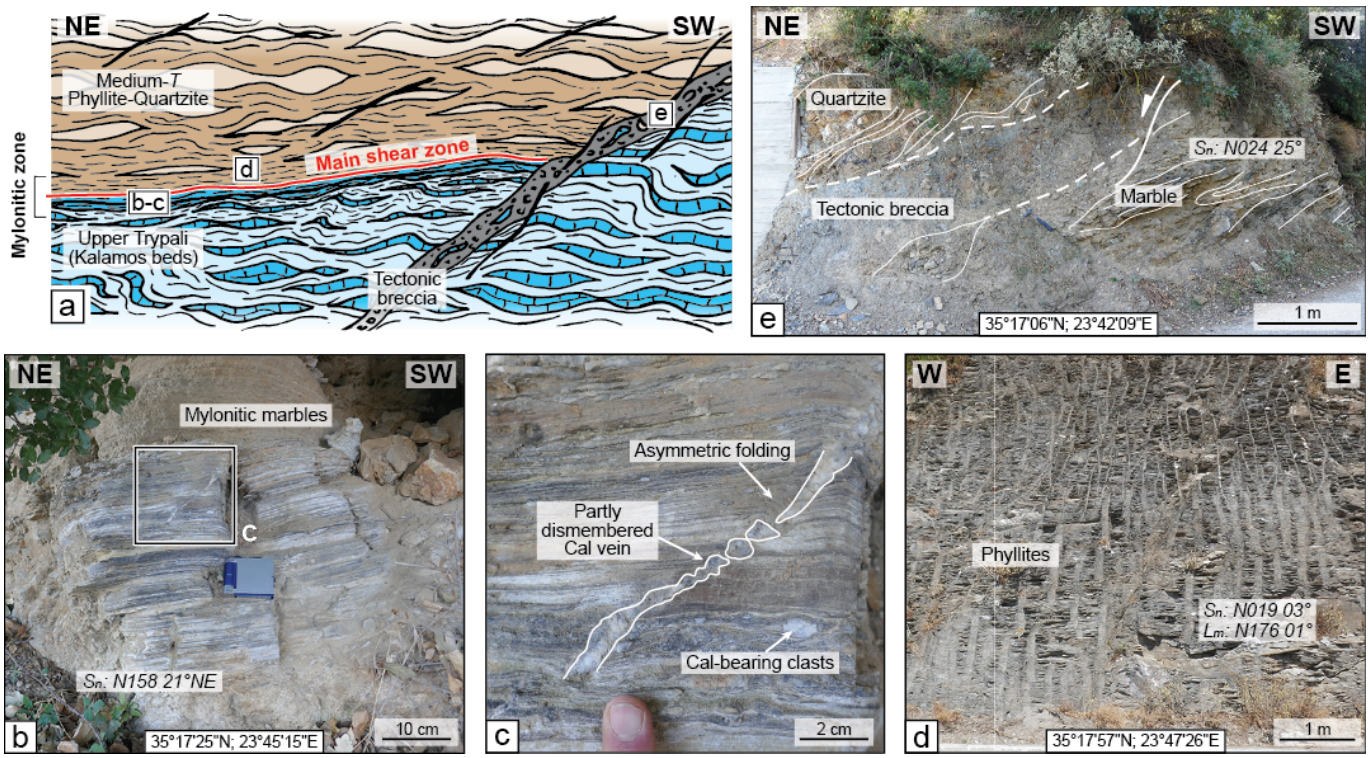

Figure 3 – Field and microscopic observations of the tectonic contacts between the tectono-metamorphic units. Main foliation measurements (*Sn*) are reported according to the right-hand rule. (**a**) Synthetic sketch showing the geometry of the contact between the Medium-*T* Phyllite-Quartzite and Upper Trypali Units. (**b**) Mylonitic marbles in the footwall of the main shear zone. (**c**) Close-up showing rounded calcite-bearing clasts and a dismembered calcite vein associated with asymmetric folding of the mylonitic foliation, indicating top-to-the-SW kinematics. (**d**) Intense schistosity in phyllitic layers from the hanging wall of the shear zone. (**e**) Tectonic breccia within the same contact, indicating late reworking.

apparent symmetrical shape are also observed in the mylonitic marble, suggesting a significant flattening component of the deformation. Further east, near the village of Agriles, the exposure of the Medium-*T* Phyllite-Quartzite Unit, a few tens of meters above the contact, shows a well-defined, nearly flat schistosity bearing a N-S-directed mineral lineation suggesting an intense deformation (Figure 3d). Subsequent reworking or truncation of this localized mylonitic shear zone is common and the contact between these two units is typically expressed as a meter-thick, moderately dipping tectonic breccia with angular clasts, predominantly of quartzite from the hanging wall and minor marble from the footwall (Figures 2b, 3e). This brittle structure is associated with secondary shear planes showing local offset of a few decimeters with apparent top-to-the-NE extensional kinematics.

Several low-angle tectonic contacts separating the H*P*-L*T* nappe stack in the footwall and the poorly metamorphosed units in the hanging wall are exposed in western Crete. Along the northern boundary of the metamorphic complex, on the crest road to the west of the Topolia Gorge, it consists of a ~6 m-thick shear zone dipping gently to moderately towards the NE at the contact between the High-*T* Phyllite-Quartzite Unit (i.e., a subdivision of the Phyllite-Quartzite *s.s.* Unit defined by thermal arguments, see Section 5) and the overlying Pindos Unit (Figures 2a, 4a). This structure is locally either sub-parallel to the metamorphic foliation of the footwall or cuts it at a moderate angle. The fault zone consists of mm- to cm-scale clasts and dm- to m-scale lenses of quartzites within a strongly deformed phyllitic matrix that has undergone hydrothermal alteration. Top-to-the-NNE shearing criteria are recognized in the fault zone, consisting of ductile-brittle S-C and S-C' structures with low- to moderate-angle extensional shear bands, respectively (Figure 4b). A few meters below the contact, the footwall exhibits an intense deformation marked by m-scale, low-angle ductile-brittle shear zones with mainly top-to-the-N kinematics, although minor top-to-the-S kinematic indicators are also observed (Figure 2a).

At the southern border of the metamorphic complex, south of the village of Kalamos, the tectonic contact with the overlying Gavrovo-Tripolitza Unit is made of a ~5 m-thick brecciated fault zone dipping gently to the south or locally to the north, following the main trend of the metamorphic schistosity in the footwall (Figures 2b, 4c-d). S-C' structures are observed in the fault zone, indicating top-to-the-S kinematics (Figure 4d). A few meters below, the Kalamos beds are affected by asymmetric recumbent folds with axial planes sub-parallel to the overlying contact, consistent with top-to-the-S kinematics.

At Cape Koutoulos, along the western coast of Crete, another low-angle tectonic contact is identified between the Rambi Seli beds (belonging to the Upper Trypali Unit) and the overlying limestones

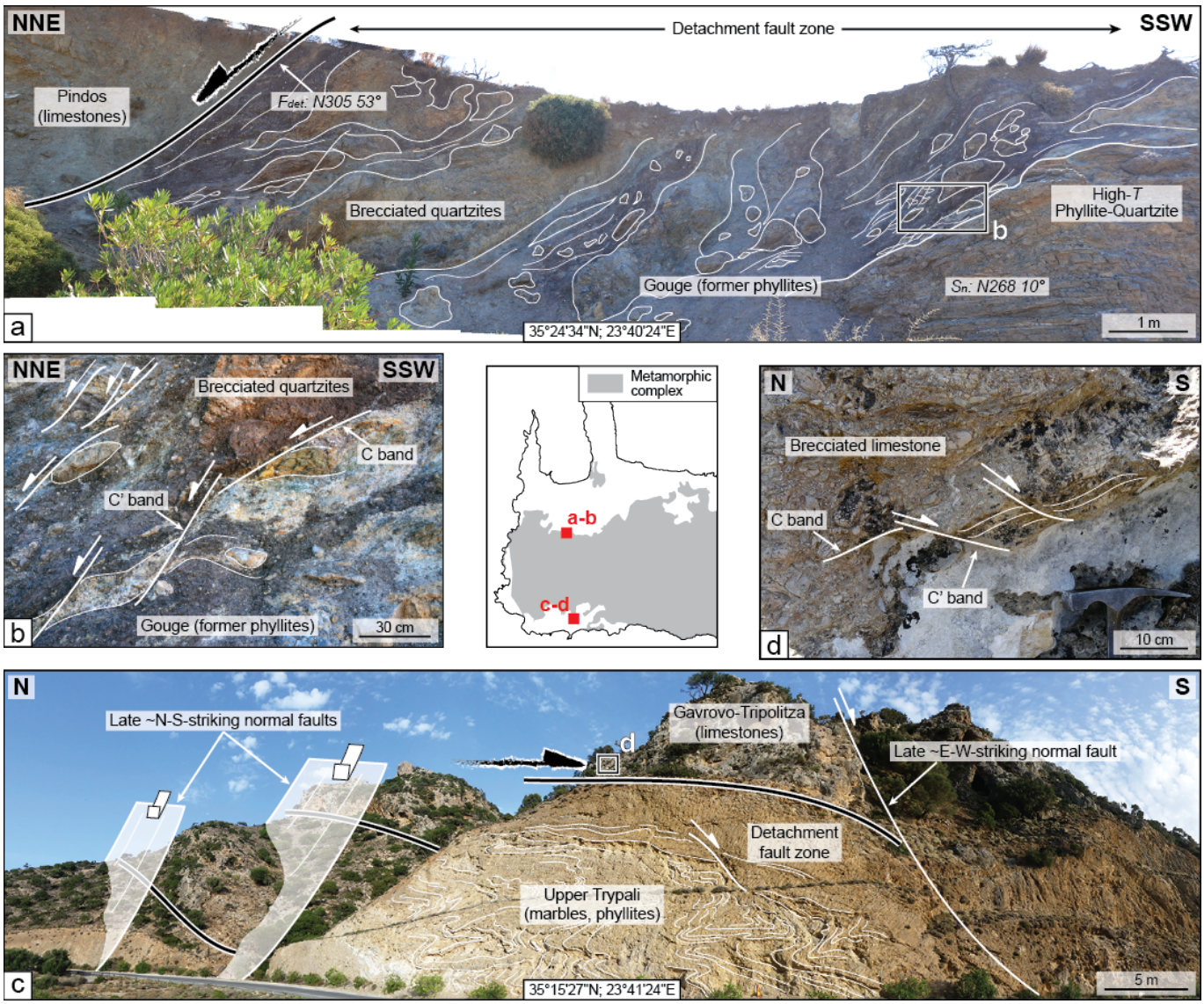

Figure 4 – Outcrops illustrating the tectonic contact between the H*P*-L*T* paleo-accretionnary complex and the overlying Upper Nappe system. These structures are interpreted as detachments (see Section 6.2). Main foliation (*Sn*) and detachment plane (*Fdet*) measurements are reported according to the right-hand rule. (**a**) N-dipping low-angle ductile-brittle extensional fault zone along the northern flank of the metamorphic nappe stack. (**b**) Close-up of the fault zone showing S-C and S-C' structures consistent with top-to-the-N kinematics. (**c**) S-dipping low-angle ductile-brittle extensional fault zone along the southern flank of the metamorphic nappe stack, dissected by late high-angle normal faults. (**d**) Close-up of the cataclastic fault zone showing S-C' structures indicating top-to-the-S kinematics (courtesy of K. Soukis).

of the Gavrovo-Tripolitza Unit (Figure 5a). This W-dipping structure consists of a ~8 m-thick fault zone, with a cataclasite composed of dark gray clasts of metaconglomerate and a hydrothermally altered brownish to yellowish fault gouge. Asymmetric deformation criteria include S-C and S-C' structures with ~N-S-striking ductile-brittle shear bands that are consistent with top-to-the-W extensional kinematics, both in the fault zone and in the footwall (Figure 5b-c).

4.2 Mesoscopic and Microscopic Structural Records

The tectono-metamorphic units of western Crete exhibit widespread ductile and brittle deformation records at outcrop scale, shedding light on the regional-scale architecture of the metamorphic complex (Figures 2, 6a). A penetrative and relatively flat schistosity ($S_{1\text{-}2}$) is well expressed in phyllitic layers and less apparent in marble and quartzitic layers. It is typically marked by phyllosilicates such as white mica and chlorite. ENE-WSW- and NNE-SSW-oriented schistosity planes, typically dipping at 10-40°, dominate the upper part of the nappe stack (i.e., the Phyllite-Quartzite *s.s.* and Upper Trypali Units), while NNE-SSW-striking planes, predominantly dipping at 40-60°, prevail in the lowermost section (i.e., from the Lower Trypali Unit down to the Gigilos beds; Figure 7a). This difference can be explained by looking at the schistosity trajectories reported on the geological map (Figure 1). Indeed, these trajectories are sub-parallel to the main contacts that trend ~E-W in the west to ~NE-SW in the east where the deepest units are exposed as a broad-scale antiform (i.e., in the Lefka Ori massif; Figure 2c). Mineral and stretching lineations ($L_{1\text{-}2}$) are occasionally visible on

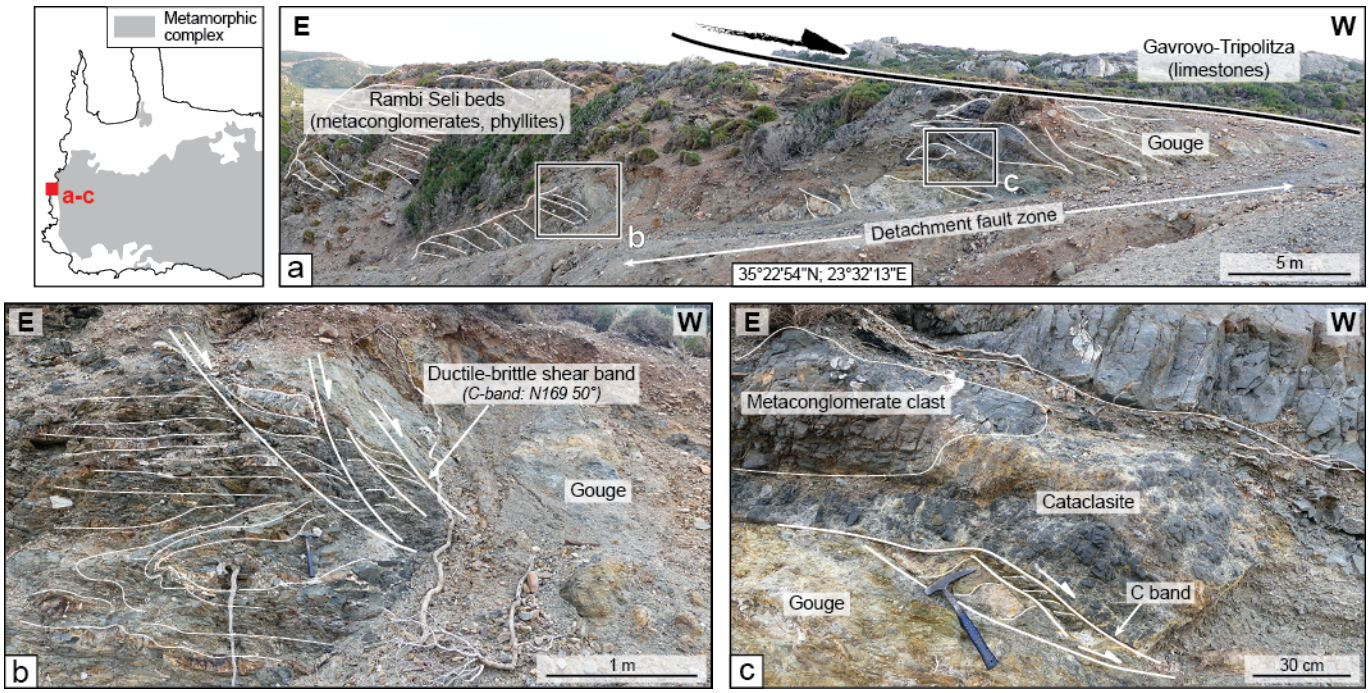

Figure 5 – Outcrop of the W-dipping ductile-brittle extensional fault zone between the Rambi Seli beds (Upper Trypali Unit) and the overlying Gavrovo-Tripolitza Unit along the western flank of the metamorphic complex. This structure is interpreted as a detachment (see Section 6.2). Shear plane measurement (*C-band*) is reported according to the right-hand rule. (**a**) General view of the outcrop. (**b**) Close-up of the footwall showing m-scale ductile-brittle extensional shear bands, indicating top-to-the-W extensional kinematics. (**c**) Close-up of the fault zone exhibiting S-C structures consistent with top-to-the-W extensional kinematics.

the schistosity planes, displaying a ~N-S orientation, evolving to NE-SW in the eastern part of the study area (Figures 1, 7b, upper panel). The lineation is generally marked by stretched quartz rods and slaty phyllosilicates and by the elongation of prismatic lawsonite and glaucophane. This planar-linear fabric likely developed close to H*P*-L*T* peak metamorphism or during early exhumation, characterized by sub-horizontal flattening and N-S- to NE-SW-directed tectonic transport.

Several generations of veins are commonly observed in the metamorphic stack with a particularly intense expression in the marble layers of the Kalamos beds belonging to the Upper Trypali Unit (Figure 6b). Millimeter-thick calcite-rich veins are commonly cut by centimeter-thick calcite-quartz veins bearing white micas, carpholite and/or lawsonite. These strongly dipping to sub-vertical veins have a ~E-W preferred orientation with H*P*-L*T* minerals growing perpendicularly to the walls (Figure 7b, lower panel). At microscopic scale, quartz and calcite show fibrous textures parallel to carpholite fibers that are occasionally crosscut by perpendicular cracks (Figure 6c). Together with intrusion trails also reported in tensile veins (see Figure S1 in Supporting Information), these observations suggest incremental crack-seal growth under H*P*-L*T* conditions and N-S oriented stretching. Some of these veins exhibit a sigmoidal shape at outcrop scale and local rotations of fibrous minerals along kink-bands at microscopic scale (Figure 6c), indicating a simple shear component with either top-to-the-N or top-to-the-S kinematics.

Intense folding is recognized in all the tectono-metamorphic units forming the H*P*-L*T* duplex in western Crete. It consists of early recumbent folds (F_1) with sub-horizontal axes predominantly oriented NE-SW (Figures 6d, 7c, upper panel) that are later affected by a second generation of open folds (F_2). The latter are characterized by sub-horizontal ENE-WSW-oriented fold axes and often exhibit an asymmetric shape, occasionally associated with minor thrust faults, suggesting apparent top-to-the-S kinematics, especially near the southern border of the metamorphic complex (Figures 2b, 6e, 7c, lower panel). Boudinage of quartzitic and marble layers in between less competent phyllites is frequent in the Phyllite-Quartzite *s.s.* and the Upper Trypali Units, supporting a significant flattening component in the deformation record (Figure 6f-g).

Ductile-brittle shear zones are observed in many places within the metamorphic rocks, crosscutting earlier folding or boudinage fabrics (Figure 6f-g). Shear planes are more or less localized and display a ~NE-SW or ~E-W orientation and a moderate dip globally comprised between 30 and 60° (Figure 7d). S-C fabrics observed in the XZ plane (i.e., parallel to the mineral or stretching lineation) and slickensides on brittle planes indicate two main kinematic settings: (i) a ~N-S- to ~NW-SE-directed, bivergent extension and (ii) a nearly perpendicular top-to-the-W shearing. It is worth noting that these two deformation records support perfectly the geometry and kinematics of the low-angle extensional structures reported on top of the nappe stack (Figures 4, 5).

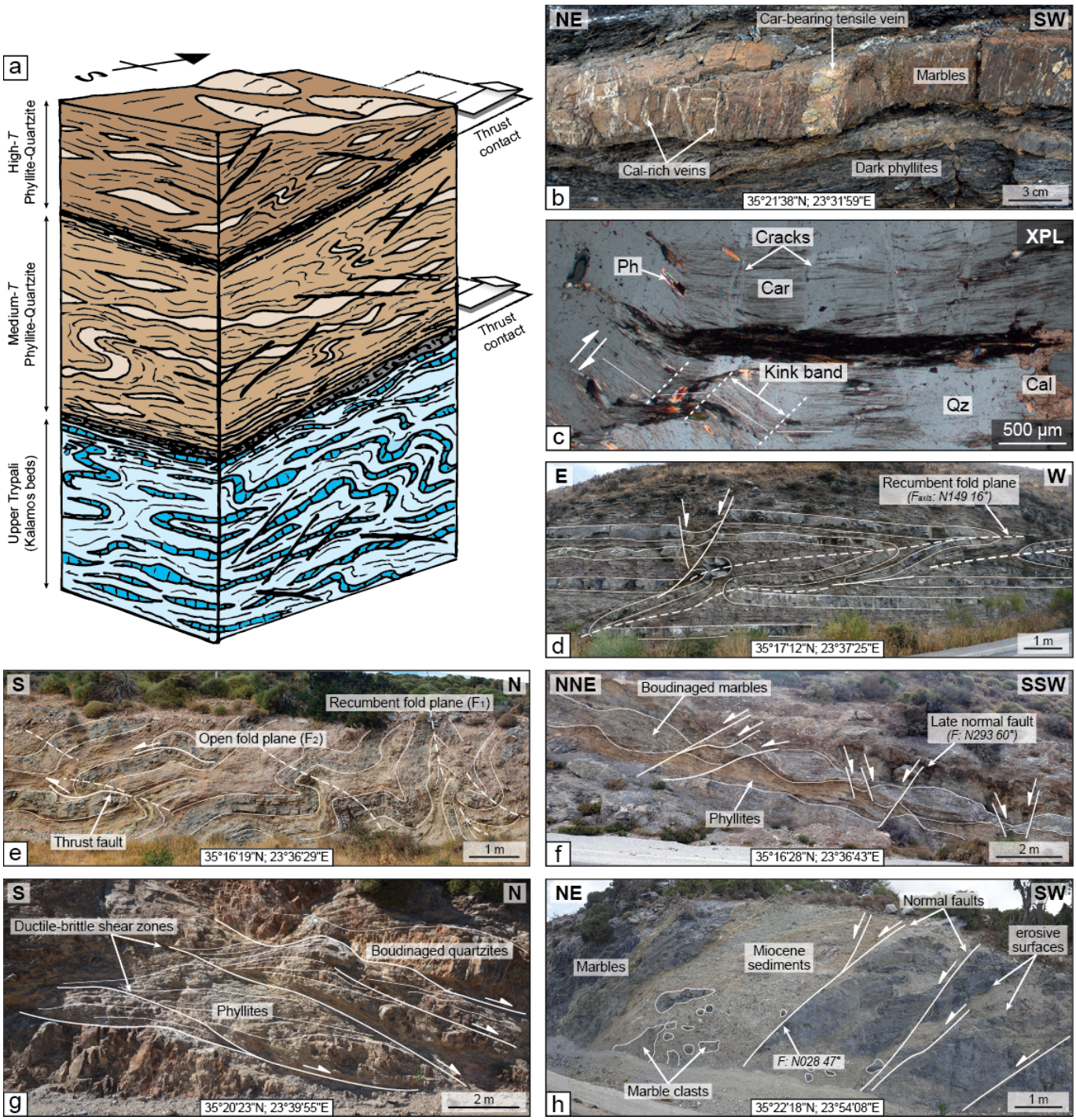

Figure 6 – Tectonic structures within the metamorphic nappe stack. Fault plane measurements (*F*) are reported according to the right-hand rule. (**a**) Synthesis of the deformation record of the tectono-metamorphic units. (**b, c**) Mesoscopic and cross-polarized-light (XPL) microscopic images of sub-vertical tensile veins with calcite (cal), quartz (qz), carpholite (car) and phengite (ph) in marble layers (Kalamos beds, Upper Trypali Unit). Carpholite fibers are perpendicular to vein walls and exhibit a crack-seal fabric and kink bands. (**d**) Recumbent folds with ~N-S-trending fold axes (Kalamos beds, Upper Trypali Unit). (**e**) Asymmetric open folds (F_2) and thrust faults reworking early recumbent folds (F_1) with apparent S vergence (Kalamos beds, Upper Trypali Unit). (**f**) Boudinage and (ductile-)brittle extensional faults (Kalamos beds, Upper Trypali Unit). (**g**) Boudinage and top-to-the-N ductile-brittle shear zones (Medium-*T* Phyllite-Quartzite Unit). (**h**) High-angle brittle normal faults in marbles (Lower Trypali Unit) with erosive surfaces and karst sediment fill.

Moderate- to high-angle brittle faults cut all the units exposed in the study area, from the Neogene-Quaternary sediments down to the base of the metamorphic complex (Figures 1, 2). These are mostly ~E-W- and N-S-oriented extensional faults cutting former ductile and ductile-brittle structures, including the major low-angle extensional shear zones at the top of the H*P*-L*T* complex (Figures 4c, 5d-f). In the eastern part of the study area, numerous m-scale brittle normal faults exhibiting a slickenside striation are observed, especially in the massive carbonates of the Lower Trypali Unit (Figure 5h). Structural measurements on these faults and calculation of the paleostress tensor using *FaultKin* software (*Marrett and Allmendinger*, 1990; *Allmendinger*

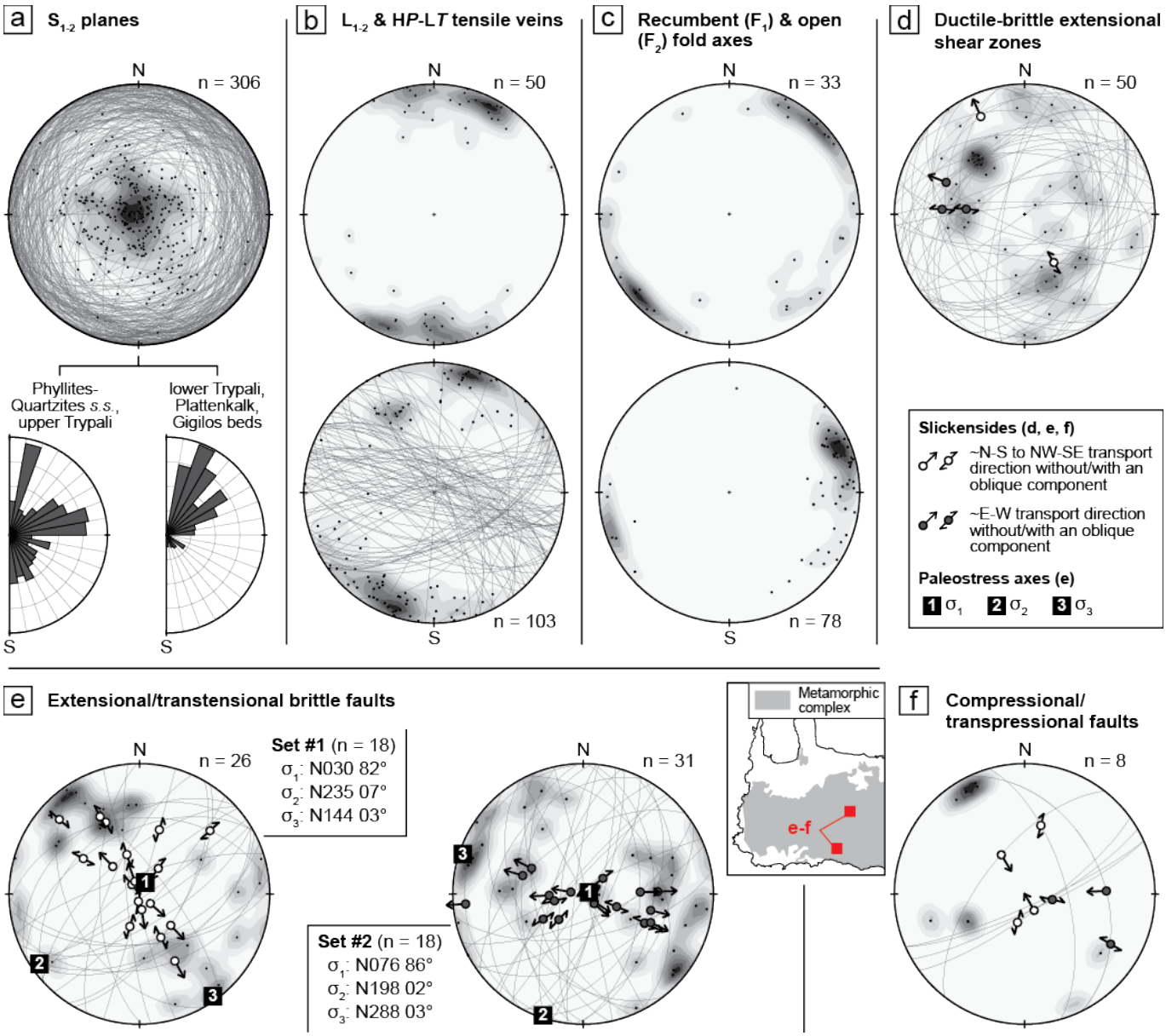

Figure 7 – Stereoplots (lower hemisphere and equal area projections) summarizing structural data from western Crete. Density contours of line features (e.g., poles of the plane, lineations or fold axes) are shown with a gray color scale. The number of measurements (n) is indicated for each plot. (**a**) S_1-S_2 schistosities (plane and pole) with rose diagrams showing the distribution of the schistosity strike in the upper (Phyllite-Quartzite *s.s.* and Upper Trypali Units) and lower (Lower Trypali Unit, Plattenkalk *s.s.* series and Gigilos beds) structural levels of the nappe stack. (**b**) L_1-L_2 lineations and H*P*-L*T* tensile veins (plane and pole), upper and lower panels, respectively. (**c**) Recumbent and open fold axes, upper and lower panels, respectively. (**d**) Ductile-brittle extensional shear zones. (**e**) Two sets of extensional and transtensional brittle faults with orientations of calculated paleo-stress axes. (**f**) Compressional and transpressional brittle faults.

et al., 2012) allow to identify two fault systems with no clear crosscutting relationship, suggesting their relative contemporaneity. The first set of normal faults are NE-SW- and E-W-oriented with a moderate to high dip between 40 and 90°. The calculated paleostress tensor is characterized by a nearly vertical σ_1 and nearly horizontal σ_2 and σ_3 oriented N235°E and N144°E, respectively. The second set of faults is roughly oriented N-S to NNE-SSW with a dip also varying between 40 and 90°. The calculated paleostress tensor then displays a nearly vertical σ_1 and nearly horizontal σ_2 and σ_3 oriented N198°E and N288°E, respectively. These two sets of faults are roughly compatible with the kinematics of the ductile-brittle shear zones reported within the metamorphic nappe stack and on top of it (Figures 4, 5, 7d), suggesting two coherent stress regimes prevailing during exhumation in the ductile-brittle then brittle crust. Finally, it is interesting to note that some reverse and transpressional brittle faults are exposed in the study area, associated with slickensides that suggest the existence of two sets of faults oriented ~ENE-WSW and ~NNW-SSE with moderate to high angle (Figure 7f).

5 RSCM Peak Metamorphic Temperatures

Peak metamorphic temperatures (T_{max}) were quantitatively estimated using the RSCM thermometry

to characterize the thermal structure of the H*P*-L*T* duplex and identify major tectonic boundaries, likely marked by significant temperature gaps.

5.1 Distribution of T_{max} Within the Nappe Stack

At first glance, analysis of the spectra shows a clear downward decrease of the organization of carbonaceous material through the metamorphic nappe stack, with a common increase of D1 and D2 defect bands relative to the G (graphite) band and, locally, the appearance of the D3 defect band, highlighting a general increase of the structural disorder within the graphitic structure (*Beyssac et al.*, 2002). Within the overlying Ravdoucha beds (i.e., corresponding to the base of the Upper Nappe system), the carbonaceous material is less organized, with spectra showing a prominent D3 band, a very large D1 band and the appearance of a D4 band, indicating low temperature peak conditions (*Lahfid et al.*, 2010).

Calculated mean values of T_{max} for all samples are reported on the geological map and cross-sections where they are expressed with their respective standard deviations (Figures 2, 8a, Table 1; see also Tables S1, S2 in Supporting Information). Considering the whole dataset, mean T_{max} embraces a relatively wide range of temperatures between ~300 °C and ~440 °C with more than half of the data distributed in the 380-410 °C interval (Figure 8b). At map scale, mean T_{max} tends to decrease from north to south and southeast, except for the two lowermost values calculated for the Ravdoucha beds, exposed in the northernmost part of the study area (Figure 8a).

By considering each unit separately, the distribution of mean T_{max} can be described as follows, from the top to the base of the nappe stack. As mentioned above, RSCM analyses in the uppermost Ravdoucha beds provide two mean T_{max} of 298 ± 15 °C and 313 ± 17 °C. In the underlying Phyllite-Quartzite *s.s.* Unit, mean T_{max} from 20 samples are distributed in two spatially coherent groups marked by a temperature step of ~15 °C, suggesting two sub-units with differing thermal histories (Figures 2a, 8a, 8c). The High-*T* Phyllite-Quartzite Unit is located in the northernmost part of the H*P*-L*T* complex and yields five mean T_{max} estimates ranging between 427 ± 9 °C and 441 ± 18 °C. This sub-unit lies above the Medium-*T* Phyllite-Quartzite Unit, largely exposed in the study area, that yields 15 mean T_{max} estimates ranging from 391 ± 12 °C to 414 ± 5 °C, excluding the value of 423 ± 20 °C where a significant component of inherited carbonaceous material is identified (Table 1; see Section 6.1). Structurally below, the Trypali Unit can also be divided in two sub-units based on their thermal imprint. The Upper Trypali Unit, which includes the Rambi Seli, Kalamos and the Stomion beds, displays 17 mean T_{max} estimates within a range between 355 ± 9 °C and 416 ± 19 °C. Note, however, that a component of inherited carbonaceous material is documented in two samples and suspected in two others that yield >400 °C mean T_{max}, all four spatially clustered near the village of Kalamos in the southern part of the study area (Figure 8a and Table 1; see Section 5.1). Only one sample from the Lower Trypali Unit, consisting essentially in carbon-poor massive marbles, has been successfully analyzed and yielded a lower mean T_{max} of 328 ± 7 °C. Finally, the underlying Plattenkalk *s.l.* Unit shows two mean T_{max} estimates of 345 ± 6 °C and 346 ± 6 °C obtained in the Plattenkalk *s.s.* series that are similar to the mean T_{max} for the Gigilos beds (i.e., 344 ± 6 °C and 350 ± 6 °C; Figures 2c, 8a).

5.2 Internal Distribution of RSCM Temperatures

When analyzing the samples individually, a unimodal T_{max} distribution is typically observed, indicating that the carbonaceous grains recorded the same maximum temperature event, corresponding to the latest and most intense peak metamorphic imprint (i.e., the subduction-related H*P*-L*T* metamorphism; see Section 6.1). This low internal dispersion of RSCM temperatures explains the small uncertainty in most of mean T_{max} (≤10 °C; Table 1). In contrast, a bimodal T_{max} distribution, observed in 16 samples, suggests an inherited component recording an older and higher thermal imprint (Figure 9). Additional spectra from six samples were acquired to further characterize this component ($n_{acquired}$ ≥27; Table 1). Two patterns emerged from the heterogeneous distribution of RSCM temperatures. In case #1 (13 samples), most spectra reflect the coldest, and youngest thermal signature, while a small fraction indicates a higher T_{max} interpreted as an inherited component (Figure 9a). These higher T_{max} spectra were discarded from the mean T_{max} calculation that reflects only the most recent thermal event. In case #2 (three samples), fewer than 10 spectra show a cold component, while most indicate a higher T_{max} (Figure 9b). Since the inherited component predominates, the mean T_{max} represents only an upper bound for the thermal imprint.

6 Discussion

Field observations, structural measurements and RSCM peak metamorphic temperatures presented in this contribution shed light on the 3D architecture of the H*P*-L*T* complex of western Crete. In the following, we first examine the significance of RSCM results and the consistency between the newly documented tectonic and thermal structures. We then discuss the first-order geometry of the tectono-metamorphic nappe stack and the succession of tectonic events related to the accretion and exhumation stages. Together, these key constraints pave the way to characterize the succession of tectono-metamorphic events and the deep accretion dynamics that took place along the Hellenic margin in the Oligocene-Miocene.

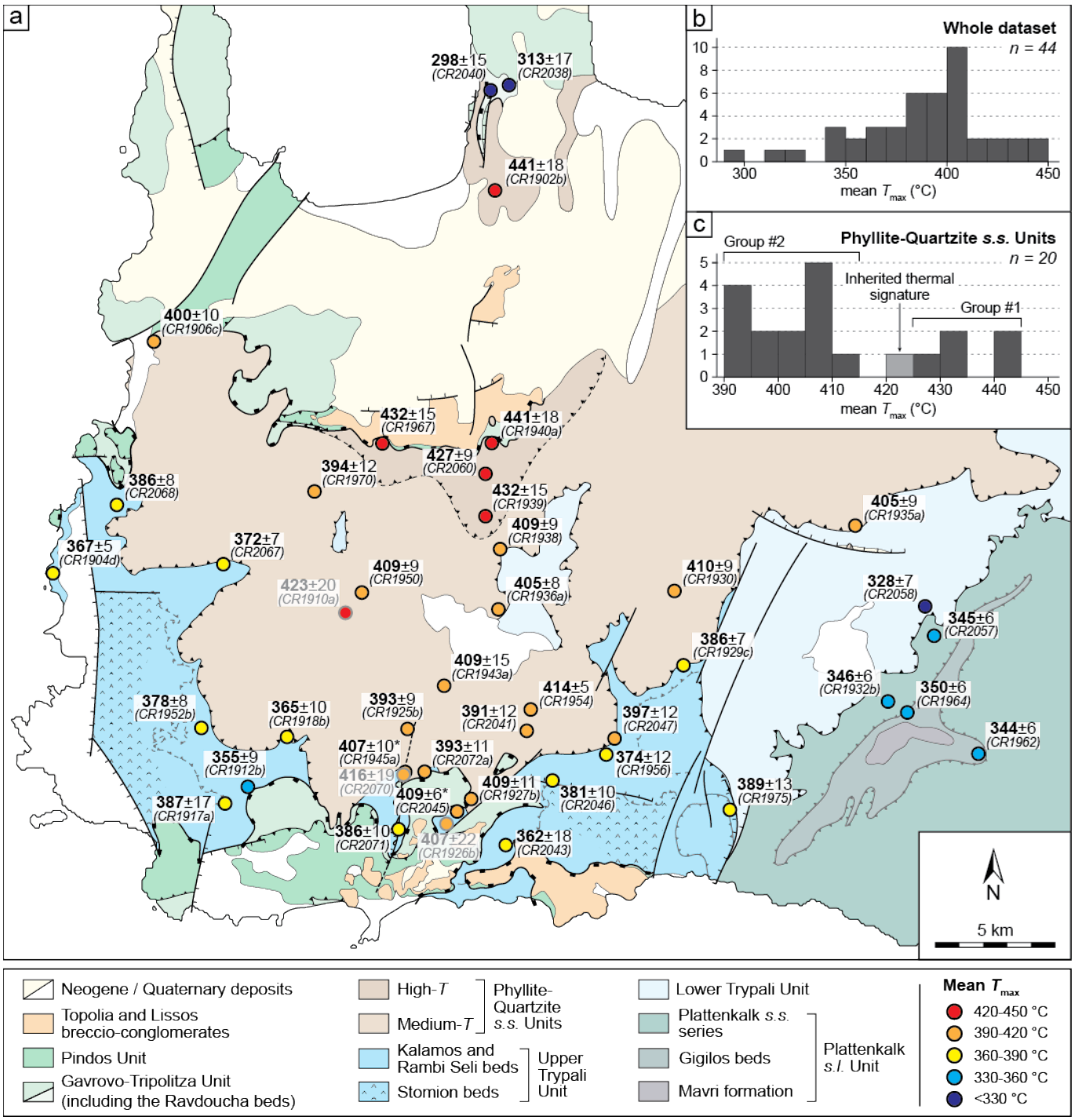

Figure 8 – The thermal structure of western Crete derived from RSCM thermometry. (**a**) Geological map showing the spatial distribution of mean T_{max} and associated standard deviations. Gray data represent mean T_{max} with a dominant inherited signature, whereas data marked with an asterisk (*) indicate mean T_{max} interpreted as inherited. Sample names are shown in italics. (**b**) Bar chart showing the distribution of mean T_{max} for the full dataset. (**c**) Bar chart showing the bimodal distribution of mean T_{max} for the Phyllite-Quartzite *s.s.* Unit, distinguishing two sub-units.

6.1 Inherited Thermal Signature and Significance of RSCM Temperatures

The RSCM temperatures reported in this study show a relatively homogeneous distribution within the tectonic units and the reconstructed thermal structure shows an overall consistency at map scale (Figures 8a, 10). However, rare instances of mean T_{max} exceeding the RSCM temperature range for a given unit are locally reported. Thus, sample CR1910a from the ~390-415 °C Medium-*T* Phyllite-Quartzite Unit yields 423 ± 20 °C, while samples CR1926b and CR2070 from the ~360-390 °C Upper Trypali Unit yield 407 ± 22 °C and 416 ± 19 °C, respectively (Table 1). These three samples exhibit a bimodal distribution of T_{max} with a dominant inherited component (Figure 9b). This implies that the mean T_{max} calculated for these samples (in gray in Figures 8, 10a) represent upper temperature bounds (case #2 in Section 5.2). Two other samples, CR1945a and CR2045, with mean T_{max} of 407 ± 10 °C and 409 ± 6 °C, respectively (Figure 9c and Table 1),

Table 1 – RSCM thermometry results. $n_{acquired}$ and n_{used} refer to the number of spectra recorded and used for mean T_{max} calculation, respectively. B and L correspond to calibration methods from *Beyssac et al.* (2002) and *Lahfid et al.* (2010), respectively. SD: Standard deviation. SE: Standard error equal to the SD divided by the square root of the number of used spectra. See Section 5.2 for details on cases #1 and #2 of thermal inheritance. P-Q: Phyllite-Quartzite.

Sample	Unit	$n_{acquired}$	n_{used}	Method	Mean T_{max} (°C)	SD	SE	Inheritance
CR1902b	High-T P-Q	20	16	B	441	18	4	
CR1904d	Upper Trypali	20	19	B	367	5	1	
CR1906c	Medium-T P-Q	20	18	B	400	10	2	
CR1910a	Medium-T P-Q	40	32	B	423	20	4	Yes (case #2)
CR1912b	Upper Trypali	20	20	B	355	9	2	
CR1917a	Upper Trypali	21	20	B	387	17	4	Yes (case #1)
CR1918b	Upper Trypali	22	19	B	365	10	2	Yes (case #1)
CR1925b	Medium-T P-Q	21	18	B	393	9	2	Yes (case #1)
CR1926b	Upper Trypali	40	37	B	407	22	4	Yes (case #2)
CR1927b	Medium-T P-Q	40	25	B	409	11	2	Yes (case #1)
CR1929c	Upper Trypali	21	21	B	386	7	2	
CR1930	Medium-T P-Q	20	20	B	410	9	2	
CR1932b	Plattenkalk s.s.	20	20	B	346	6	1	
CR1935a	Medium-T P-Q	20	19	B	405	9	2	
CR1936a	Medium-T P-Q	20	20	B	405	8	2	
CR1938	Medium-T P-Q	23	21	B	409	9	2	Yes (case #1)
CR1939	High-T P-Q	23	13	B	432	15	4	
CR1940a	High-T P-Q	20	19	B	441	18	4	
CR1943a	Medium-T P-Q	20	18	B	409	15	4	Yes (case #1)
CR1945a	Upper Trypali	40	36	B	410	10	2	Yes (case #1)
CR1950	Medium-T P-Q	21	21	B	409	8	2	
CR1952b	Upper Trypali	22	21	B	378	8	2	
CR1954	Medium-T P-Q	21	20	B	414	5	1	
CR1956	Upper Trypali	20	18	B	374	12	3	Yes (case #1)
CR1962	Gigilos beds	21	20	B/L	344	6	1	
CR1964	Gigilos beds	20	20	B/L	350	6	1	
CR1967	High-T P-Q	22	22	B	432	15	3	
CR1970	Medium-T P-Q	24	24	B	394	12	3	
CR1975	Upper Trypali	20	18	B	389	13	3	Yes (case #1)
CR2038	Ravdoucha beds	19	19	L	313	17	4	
CR2040	Ravdoucha beds	20	20	L	298	15	3	
CR2041	Medium-T P-Q	20	20	B	391	12	3	
CR2043	Upper Trypali	20	20	B	362	18	4	
CR2045	Upper Trypali	27	21	B	409	6	1	Yes (case #1)
CR2046	Upper Trypali	22	20	B	381	10	2	Yes (case #1)
CR2047	Medium-T P-Q	20	18	B	397	12	3	
CR2057	Plattenkalk s.s.	22	20	B	345	6	1	
CR2058	Lower Trypali	20	16	L	328	7	2	
CR2060	High-T P-Q	20	20	B	427	9	2	
CR2067	Upper Trypali	22	22	B	372	7	1	
CR2068	Upper Trypali	32	26	B	386	8	2	Yes (case #1)
CR2070	Upper Trypali	18	14	B	416	19	5	Yes (case #2)
CR2071	Upper Trypali	22	20	B	386	10	2	Yes (case #1)
CR2072a	Medium-T P-Q	22	20	B	393	11	3	

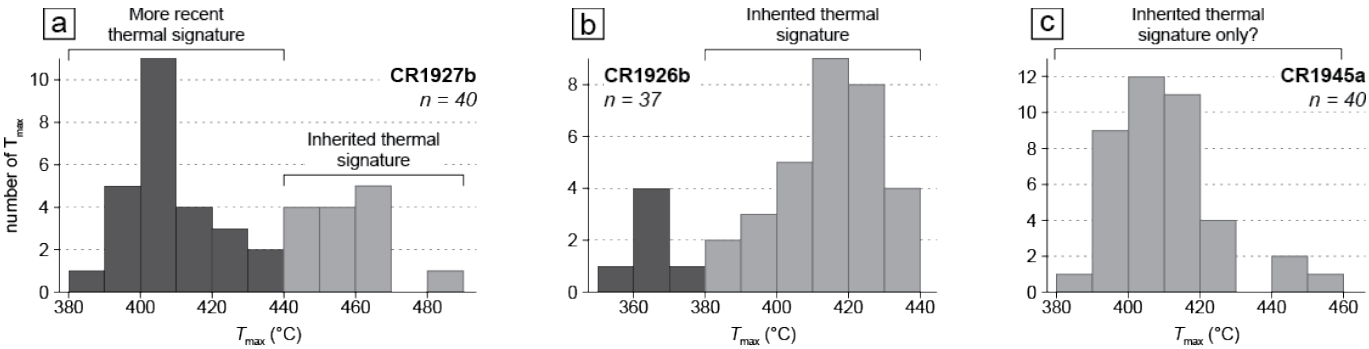

Figure 9 – Bar charts illustrating the bimodal distribution of T_{max}, revealing an inherited thermal signature in analyzed samples. (**a**) Subsidiary inherited thermal signature allowing an accurate estimate of mean T_{max} (case #1). (**b**) Dominant inherited thermal signature permitting only an upper bound estimate for mean T_{max} (case #2). (**c**) Specific T_{max} distribution showing an inherited thermal signature only, inferred from RSCM temperatures and T_{max} dispersion in nearby samples (see Section 6.1).

also merit further discussion. These samples both belong to the Upper Trypali Unit that typically shows mean T_{max} ranging between ~360 and 390 °C (Figure 10a). Additionally, the main T_{max} component of these samples is similar to the dominant inherited thermal signature of nearby samples CR1926b and CR2070 (i.e., compare Figure 9b and c). This suggests that CR1945a and CR2045 only record the thermal inheritance and, thus, we interpret their T_{max} as maximum temperature bounds. Alternatively, the clustered >400 °C mean T_{max} observed in the Upper Trypali Unit (Figures 8a, 10) might indicate a deeper, warmer section of this metamorphic nappe that has been locally exposed near the village of Kalamos (Figure 8a).

After removing the influence of the inherited thermal component of carbonaceous matter, the geological significance of the thermal imprint recorded in the tectonic units can be discussed. All Raman measurements from the metamorphic complex were conducted on metasediments with protolith ages ranging from late Carboniferous to Eocene (*Krahl et al.*, 1983; *Soujon et al.*, 1998; *Zulauf et al.*, 2018). This indicates that the unique thermal event recorded by these rocks is related to the subduction of the Gavrovo-Tripolitza and the Ionian platforms during the Oligocene-middle Miocene (*Bonneau*, 1984; *Jolivet and Brun*, 2010; *Papanikolaou and Vassilakis*, 2010). Accordingly, the RSCM results are consistent with previously published *P-T* estimates for H*P*-L*T* metamorphism in western Crete. For example, the Phyllite-Quartzite *s.l.* Unit exhibits peak conditions of 10 ± 3 kbar and 400 ± 50 °C (*Theye et al.*, 1992) that are compatible with the calculated mean T_{max} comprised between 355 ± 9 °C and 441 ± 18 °C (excluding the 328 ± 7 °C calculated in the Lower Trypali Unit). Similarly, the *P-T* conditions of >7 kbar and 350-400 °C documented for the Plattenkalk *s.l.* Unit (*Seidel et al.*, 1982) align with the RSCM results ranging between 344 ± 6 °C and 350 ± 6 °C. This overall consistency also suggests that the RSCM peak metamorphic temperature was coeval (or near coeval) with the peak pressure and that no significant heating occurred during subsequent exhumation. This interpretation is notably supported by retrograde *P-T* paths for the Phyllite-Quartzite *s.l.* Unit in western Crete that show either cooling or only minor heating during decompression (*Jolivet et al.*, 1996; see also the companion paper for new P-T paths: *Menant et al.*, 2026, this issue).

Several previous studies also report RSCM temperatures from the study area. *Rahl et al.* (2005) proposed a revised calibration of the RSCM thermometer of *Beyssac et al.* (2002) and calculated temperatures for the Phyllite-Quartzite *s.l.* Unit ranging from 260 °C to 448 °C, as well as two temperatures for the Plattenkalk *s.l.* Unit (266 °C and 291 °C). While there is notable variability in these estimates, they are generally consistent with our data when accounting for the ±50 °C uncertainty on absolute-temperature calculation. However, Rahl *et al.* (2005) did not find spatial consistency in the distribution of RSCM temperatures across western Crete, preventing the identification of a distinct thermal signature corresponding to the tectono-metamorphic units observed in the field. Additionally, *Klein et al.* (2013) obtained RSCM temperatures from the Upper Nappe system and the Phyllite-Quartzite *s.l.* Unit, using two calibrations (*Beyssac et al.*, 2002; *Rahl et al.*, 2005). While some of their results are in partial agreement with our data, their measurements are associated with relatively high uncertainty (i.e., standard deviations of 40–73 °C for Rahl's calibration and 17-29 °C for Beyssac's calibration). The presence of an inherited carbonaceous component in over a third of our analyzed samples (Table 1) and the significant uncertainty on calculated temperatures likely explain the discrepancies between our dataset and those of prior works.

In conclusion, the close alignment between our RSCM peak metamorphic temperatures and *T* estimates from previous petro-metamorphic studies (*Seidel et al.*, 1982; *Theye et al.*, 1992; *Jolivet et al.*, 1996), combined with the extensive sampling and the spatial consistency of the dataset, strongly supports the validity of the reconstructed thermal structure (Figures 8a, 10a). This structure can now be evaluated in the context of the first-order tectonic structures observed in the field.

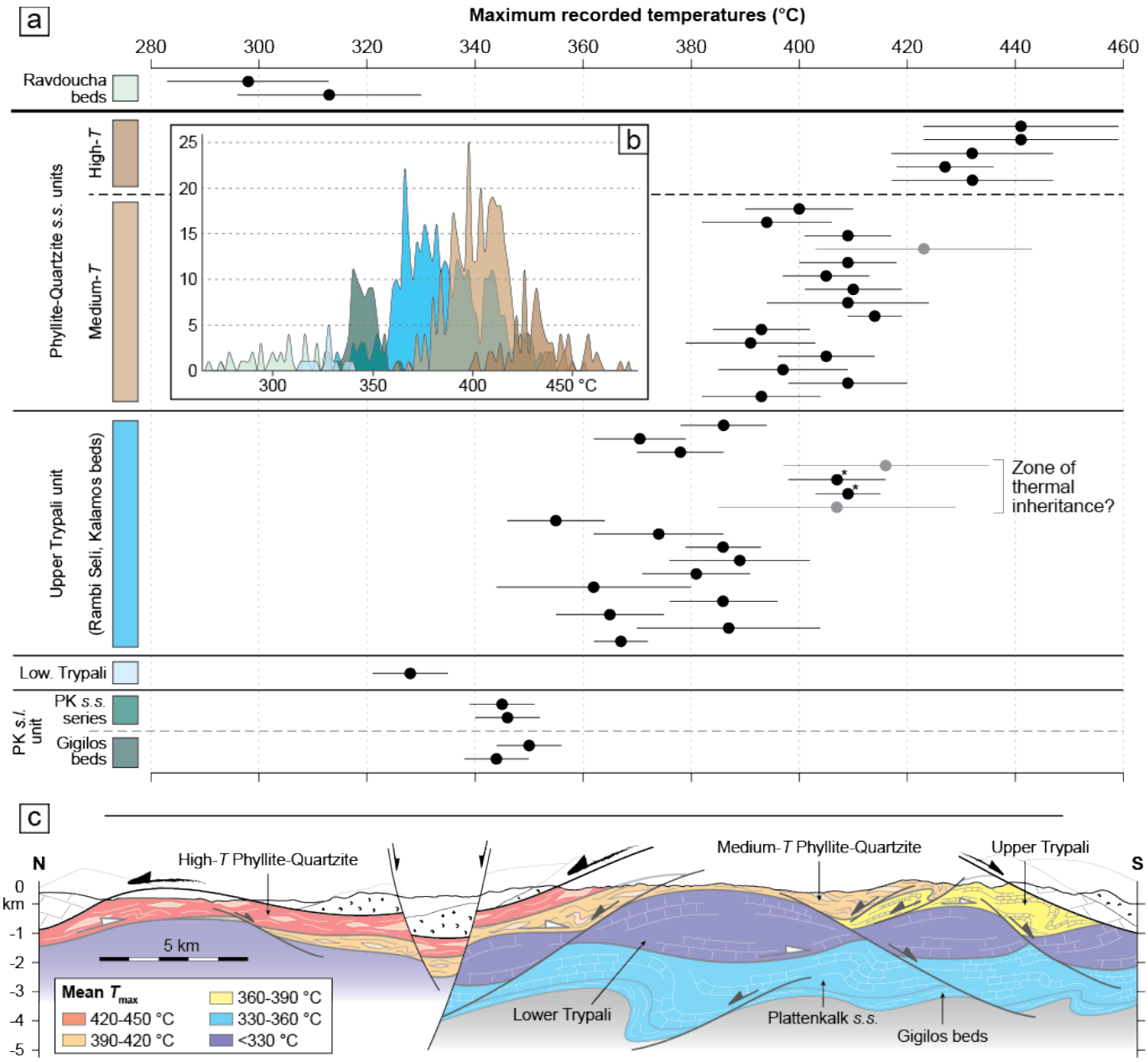

Figure 10 – The thermal signature of the tectonic units derived from RSCM temperatures. (**a**) Distribution of mean T_{max} and associated standard deviations within the poorly-metamorphosed and H*P*-L*T* units. Gray data represent mean T_{max} with a dominant inherited signature, whereas data marked with an asterisk (*) indicate mean T_{max} interpreted as inherited. PK: Plattenkalk. (**b**) Distribution of T_{max} calculated from individual Raman spectra for each tectono-metamorphic unit, excluding data influenced by an inherited thermal signature. (**c**) Synthetic 2-D cross-section of western Crete with H*P*-L*T* units colored according to their T_{max} range.

6.2 Kinematics of Main Tectonic Contacts and Consistency with the Thermal Structure

Some of the most prominent tectonic structures recognized in western Crete mark the contact between the subduction-related H*P*-L*T* complex in the footwall and the poorly metamorphosed Upper Nappe system in the hanging wall. Newly reported key outcrops of this contact document meter- to decametre-thick low-angle shear zones exhibiting ductile-brittle deformation (Figures 4, 5). Apparent extensional shearing criteria are systematically observed within the fault zones that exhibit top-to-the-N, top-to-the-S- and top-to-the-W kinematics along the northern, southern and western flanks of the metamorphic complex, respectively. Along with the recognition of a significant pressure gap (i.e., ~10 kbar) (*Jolivet and Brun*, 2010), this major contact also exhibits a temperature gap that can reach more than 100 °C, as evidenced by the RSCM peak metamorphic temperatures recorded in the Ravdoucha beds (i.e., the hanging wall) and in the High-*T* Phyllite-Quartzite Unit (i.e., the footwall); i.e., ~290-330 °C and ~420-460 °C, respectively (Figure 10). *Rahl et al.* (2005) reported a lower break in the RSCM temperatures along this tectonic contact in central and eastern Crete that is consistent with the eastward decrease of peak metamorphic temperatures documented in Crete (*Seidel et al.*, 1982; *Theye et al.*, 1992). Structural observations

combined with P-T records allow us to interpret these contacts as detachments, in agreement with other studies from the same area (*Jolivet et al.*, 1994, 1996; *Papanikolaou and Vassilakis*, 2010) and from central and eastern Crete (*Fassoulas et al.*, 1994; *Jolivet et al.*, 1996; *Ring et al.*, 2001; *Grasemann et al.*, 2019) that identified one or two main structures with dominant top-to-the-N kinematics or bivergent N-S-striking kinematics. It is noteworthy that three detachments are now mapped in western Crete as they include the top-to-W low-angle extensional shear zone at Cape Koutoulos reported for the first time in this study (Figures 1, 5). These structures likely played a significant part to the unroofing of the metamorphic complex in the Miocene (*Jolivet et al.*, 1996; *Ring et al.*, 2001), coevally with the deposition of supra-detachment basins (*van Hinsbergen and Meulenkamp*, 2006; *Seidel et al.*, 2007). Their activity was probably diachronous, depending on the dominant stress regime in the crust (see Section 6.4).

It is worth mentioning that asymmetric deformation indicators in the footwalls of the detachments occasionally show an opposed sense of shear compared to the main shear zone. S-C structures with top-to-the-S kinematics are thus reported immediately below the top-to-the-N detachment along the northern border of the metamorphic complex (Figure 2a; see also Figure 9 in *Chatzaras et al.* (2013)). This observation might explain the contrasting interpretation of this major structure as a top-to-the-S out-of-sequence thrust fault in western Crete (i.e., the so-called Tripolitsa thrust) (*Chatzaras et al.*, 2013) that is at odds with the kinematic indicators observed in the core of the detachment fault (Figure 4a-b) and fails to explain the pressure and temperature gap and the ~30 km thickness of missing crust across this contact (Figure 10a) (*Jolivet et al.*, 2010) that are, instead, typical of detachment faults reported in mountain belts worldwide (e.g., *Lister and Davis*, 1989; *Jolivet et al.*, 1998). This deformation record rather suggests a significant component of coaxial strain under an extensional stress regime associated with an intense stretching of the crust. Non-coaxial deformation accommodating the exhumation of the metamorphic stack was then extremely localized along the detachments, suggesting an activation of these large-scales structures in a relatively cold crust (i.e., just above an active subduction zone).

Other significant tectonic structures in western Crete mark the contact between the stacked tectono-metamorphic units constituting the HP-LT complex. Although they are often reworked or truncated by late normal faults, these structures occasionally preserve an early mylonitic fabric with top-to-the-SW shear indicators supporting an intense and localized deformation in the ductile regime, likely under HP-LT conditions (Figure 3; see also the companion paper for new geochronological constraints on the early activity of these contacts: *Menant et al.*, 2026, this issue). In agreement with literature (*Papanikolaou and Vassilakis*, 2010; *Chatzaras et al.*, 2013), these major structures are interpreted as early compressional shear zones with a southward vergence that accommodated the slicing of the metamorphic nappes and their accretion to the base of the forearc domain. The importance of these tectonic boundaries is further supported by the reconstructed thermal structure that shows a well-resolved down-stepping of the measured RSCM temperatures towards the base of the exposed metamorphic nappe stack (Figure 10c). Thus, a temperature step comprised between 15 and 30 °C; i.e., higher than the relative uncertainties on the RSCM measurements (*Beyssac et al.*, 2004), characterizes each contact and indicates contrasting thermal histories for the tectono-metamorphic units. These units include the Plattenkalk *s.l.* Unit that encompasses the Plattenkalk *s.s.* series and the Gigilos beds as they yield similar T_{max}. Given that the peak metamorphic temperature was likely coeval (or near coeval) to the peak pressure for all the tectono-metamorphic units (see Section 6.1), there are two explanations for the decreasing RSCM temperatures towards the base of the nappe stack; i.e., towards the more recently accreted unit. Either the subduction zone cooled through time or the depth of basal accretion decreased stepwise with every tectono-metamorphic unit to lower P-T peak conditions. Evaluating these two alternatives is hampered as the pressure peak reported in the literature is not adequately resolved (i.e., ranging between ~10 and ~18 kbar in the Phyllite-Quartzite *s.l.* Unit in western Crete) (*Theye et al.*, 1992; *Jolivet et al.*, 1996). To tackle this issue, finer P-T estimates, combined with precise dating of the accretion and exhumation stages for the different tectonic units, are presented in the companion paper (*Menant et al.*, 2026, this issue).

From a broader perspective, the ~350-450 °C mean T_{max} obtained for the metamorphic nappe stack in western Crete falls within the temperature range estimated for the downdip end of seismogenic zones worldwide (*Oleskevich et al.*, 1999). This transitional zone corresponds to either the brittle-ductile transition in crustal rocks or the intersection with the overriding plate Moho or a combination of both. This notable correspondence suggests a first-order thermo-mechanical control on the depth of basal accretion along the subduction interface that likely aligns with the downdip limit of the seismogenic zone (*Agard et al.*, 2018; *Menant et al.*, 2019).

6.3 A Dome-like Duplex Structure

New field observations and RSCM measurements presented in this study, combined with lithostratigraphic, structural and radiometric data compiled from literature, allowed to identify a minimum of five tectono-metamorphic units bounded by major ductile-brittle shear zones exhibiting a top-to-the-S reverse kinematics that is commonly overprinted by tectonic reworking (Figures 2, 3) and yields differing RSCM temperature records (Figures 10, 11). From the top to the base, the nappe succession is described as follows: the High-T and Medium-T Phyllite-Quartzite Units, the Upper and Lower Trypali Units and the Plattenkalk *s.l.* Unit. Note, however, that

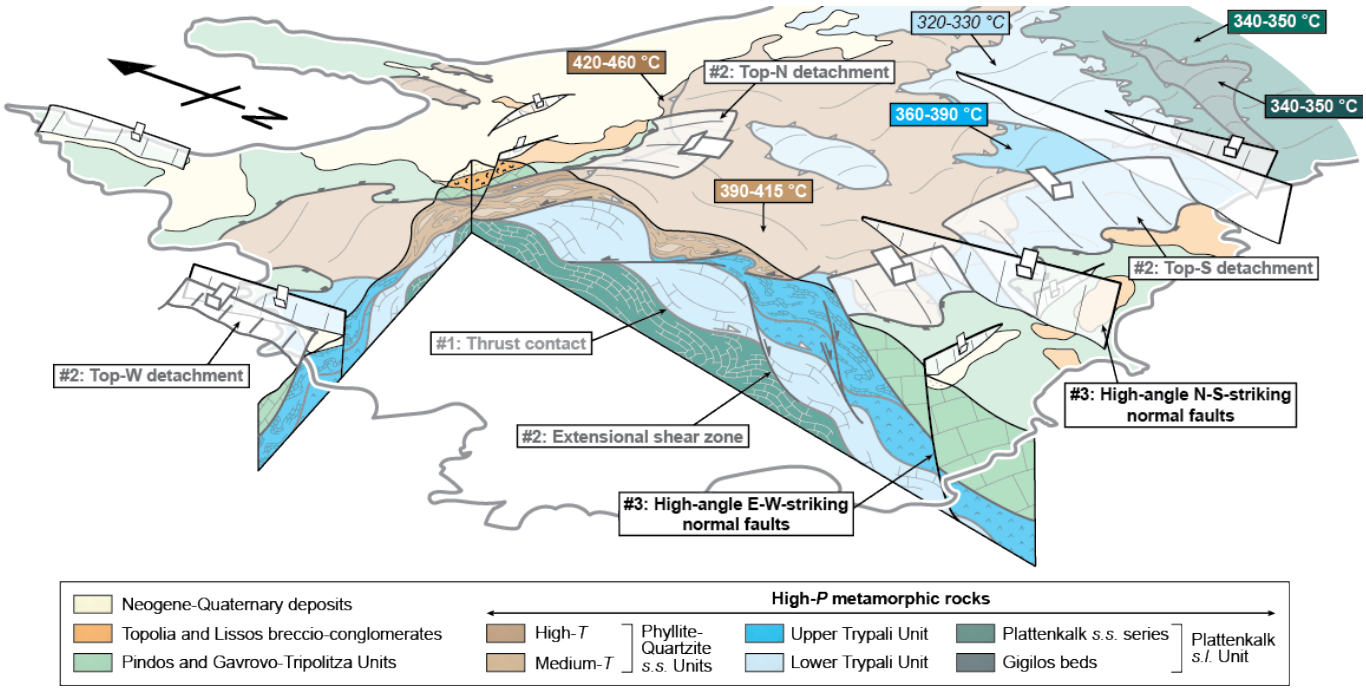

Figure 11 – First-order geometry of the H*P*-L*T* duplex and the overriding Upper Nappe system. T_{max} ranges for each tectono-metamorphic unit are indicated. The main tectonic structures, with labels colored light gray, dark gray and black colors, correspond to tectonic events #1, #2 and #3, respectively (see Section 6.4).

additional units might have been overlooked, especially if they share similar lithostratigraphic or metamorphic characteristics, or totally omitted because of the late reworking of major tectonic contacts. This tectonic architecture does not support the sub-division of the Upper and Lower Phyllite-Quartzite Units as proposed by *Ring et al.* (2022), questioning the nature of the intra-Phyllite-Quartzite thrust fault. Thus, although we cannot totally discard the existence of a diffuse high-strain zone in this area (see Figure 5 in *Ring et al.*, 2022), it should not be considered as a major tectonic contact bounding two distinct tectono-metamorphic nappes.

Relatively flat schistosity ($S_{1\text{-}2}$) mapped at the scale of western Crete suggests that the whole nappe stack forms a first-order dome-like structure, called hereafter "duplex", affected by subsidiary geometric complexities (Figures 1, 7a). These complexities are characterized by curved schistosity trajectories on map projection with N-S- and NE-SW-oriented axial planes in the western and eastern parts of the metamorphic complex, respectively. These undulations can be explained by km-scale folding and/or boudinage of the duplex that are both reported at mesoscopic scale (Figure 6d-f). The similar orientation of these map-scale structures and the mineral and stretching lineations ($L_{1\text{-}2}$) supports the interpretation of km-scale elongated boudins. Conversely, F_2 folding (i.e., syn- to post-S_2 schistosity) displays axial planes that are generally oriented E-W, NE-SW or NW-SE (Figure 7c, lower panel), which is only partly consistent with the mapped schistosity trajectories. Thus, although we acknowledge that boudinage and folding both contributed to the large-scale geometry of the duplex in western Crete, we propose that the finite structure is dominated by boudinage of more competent layers (i.e., quartzites or marble) that developed by combined constriction and flattening during the exhumation and thinning of the nappe pile (Figures 2, 11) (*Fassoulas et al.*, 1994; *Jolivet et al.*, 1994, 1996).

There is no systematic lateral continuity in the succession of the tectono-metamorphic units. For example, the Upper Trypali Unit is not observed in the northern part of the metamorphic domain where the Medium-*T* Phyllite-Quartzite Unit directly lies on top of the massive marbles of the Lower Trypali Unit (Figures 1, 2a, 11). The asymmetric shape of the duplex may have developed early during its formation, as accreted tectonic slices could have originally had significantly different spatial extents. Alternatively, sections of the tectono-metamorphic units may have been removed during late-stage reworking of major tectonic contacts during the exhumation of the nappe stack. This would suggest more intense extensional shearing and stretching in the northern part of the duplex, implying a greater displacement along the top-to-the-N detachment compared to its top-to-the-S counterpart. It is also plausible that the interplay between the two processes contributed to the duplex asymmetry, as exhumation-related deformation may have been partly controlled by the original extent of the accreted tectonic slices.

Finally, the progressive rotation of schistosity trajectories, accompanied by mineral and stretching lineations in a NE-SW direction may be linked to the surface exposure of the deepest portion of the duplex that forms a broad antiform oriented in the same direction (Figures 1, 2c). This is consistent with the NW-SE-directed extensional kinematics of brittle faults

reported in this area (Figure 7e, left panel), suggesting that this map-scale structure formed during the exhumation of the nappe stack in the ductile-then-brittle forearc crust. *Chatzaras et al.* (2013) interpreted this region as a crustal-scale oblique ramp, originating from an inherited Mesozoic fault zone belonging to the subducting Gavrovo-Tripolitza and Ionian platforms. However, the supposed syn-sedimentary extensional faults supporting their hypothesis are here interpreted as ductile-brittle extensional shear zones that affected the subduction-related H*P*-L*T* assemblage (Figure 6f-g). Field evidence for tectonic structures formed prior to subduction remains, therefore, elusive and likely difficult to identify due to the tectonic and metamorphic overprint during the basal-accretion and exhumation stages.

6.4 Accretion-then-exhumation Sequence: Deformation Timescales

This study provides constraints on the succession of deformation events recorded by the metamorphic duplex in western Crete during its journey from the subduction interface to the forearc upper crust. The deformation record of the successive basal-accretion events includes south-vergent ductile shear zones, acting as km-scale thrusts that accommodated the stacking of the tectonic slices and the sequential growth of the duplex (see structures from tectonic event #1 in Figure 11). Associated recumbent folding with fold axis that tends to align with the N-S- to NE-SW-trending L_1 lineation indicates a significant trench-perpendicular stretching during the basal accretion events in the Oligocene-early Miocene (Figures 6c, 7b-c) (*Fassoulas et al.*, 1994; *Jolivet et al.*, 1996). Coevally, ~E-W-striking tensile veins bearing carpholite and/or lawsonite growing perpendicular to the walls were formed. They typically exhibit a crack-seal fabric suggesting successive stages of fracture opening and precipitation under H*P*-L*T* conditions and near-lithostatic pore fluid pressures (Figure 6b-c) (Ramsay, 1980).

The subsequent exhumation stage is characterized by a roughly constant N-S-trending L_2 stretching lineation, widespread boudinage and greenschist-facies ductile-brittle shear zones that contributed to the thinning of the tectono-metamorphic units during a ~N-S-directed crustal extension (Figures 6f-g, 7b, upper panel) (*Fassoulas et al.*, 1994; *Jolivet et al.*, 1994, 1996). The coeval activity of the top-to-the-N and top-to-the-S detachments contributed to the exhumation and doming of the duplex across the forearc crust during the early-middle Miocene (*Thomson et al.*, 1998; *Marsellos et al.*, 2010), with the top-to-the-N structure likely dominating (see structures from tectonic event #2 in Figure 11). This trench-perpendicular extensional stress regime did not prevail during the entire exhumation stage. Indeed, the newly reported top-to-the-W detachment and N-S-oriented shear zones active in the ductile-brittle field both indicate a ~E-W-directed (i.e., trench-parallel) extension that likely developed, at least intermittently, from the progressive bending of the subduction zone during its fast retreat towards the south in the middle-late Miocene (Figures 5, 7d, 11) (*Armijo et al.*, 1992; *van Hinsbergen and Meulenkamp*, 2006; *Marsellos et al.*, 2010). The final exhumation of the duplex is associated with two main sets of high-angle brittle normal faults, oriented ~E-W to NE-SW and ~N-S, that crosscut all previous structures (see structures from tectonic event #3 in Figure 11). This supports the protracted nature of the N-S- and E-W-directed extensional events that have likely alternated up to the present, as indicated by the recent activity of similarly oriented structures (*Nicol et al.*, 2020).

Although extensional deformation prevails in Crete, ductile and brittle structures compatible with compressional and transpressional events are also reported (*Chatzaras et al.*, 2006, 2013; *van Hinsbergen and Meulenkamp*, 2006; *Tortorici et al.*, 2010; *Ring and Yngwe*, 2018). The latter include asymmetric open folds with a southward vergence and two sets of reverse and transpressional faults, oriented ~N-S to NW-SE and E-W, that are observed locally in western Crete (Figures 6d, 7f). Whereas the ductile structures could develop under H*P*-L*T* conditions during deep nappe stacking, brittle structures were formed in the forearc upper crust, suggesting successive periods of dominant extension and compression/transpression from the middle Miocene to recent times. Similarly, *Zulauf et al.* (2002) proposed several changes of stress regimes during the formation and exhumation of the metamorphic duplex in Crete due to the modification of the far-field force balance over Myr timescales. However, since no clear chronology can be established between these contradictory deformation regimes recorded in both the ductile and the brittle crust, one alternative hypothesis is that the different stress regimes succeed each other on much shorter timescales. Indeed, seismic and geodetic monitoring at active margins has shown that forearc crust records composite fault patterns, accompanied by varying seismic and aseismic deformation styles, that develop due to local stress field perturbations during the seismic cycle (*Shirzaei et al.*, 2012; *Mouslopoulou et al.*, 2020). Thus, variation in stress regime at tens-to hundreds-yr-scale could explain the complex structural records observed in western Crete, as well as the difficulty in establishing a clear chronology of the tectonic events recorded in the metamorphic duplex during its exhumation through the ductile and brittle forearc crust. For instance, south-vergent mylonitic thrusts and ~E-W-striking H*P*-L*T* tensile veins with crack-seal fabrics both formed near the basal-accretion site (Figures 3b, 6b-c, 7b). These structures may reflect contrasting stress regimes along the deep subduction interface; i.e., a compressional regime with a N-S-oriented σ_1 for the thrusts and an extensional regime with a N-S oriented σ_3 for the veins. This apparent contradiction could be explained by short-term fluctuations in stress regime, as discussed above. However, under H*P*-L*T* conditions where ductile deformation prevails, reconstructing the stress field and determining whether such stress regimes are regional or localized remains a significant challenge. Addressing this issue requires detailed structural analysis in

paleo-duplexes worldwide, combined with investigations of both long- and short-term stress evolution predicted by physically-based modeling.

7 Conclusion

This study provides new field observations, structural measurements and RSCM analyses that illuminate the 3D tectonic and thermal architecture of the H*P*-L*T* duplex exposed in western Crete. A minimum of five tectono-metamorphic units have been identified, each characterized by a distinct thermal signature, suggesting that they correspond to different episodes of basal accretion along the Hellenic-subduction interface during the Oligocene-Miocene. The ductile shear zones locally preserved at the contacts between these accreted slices are pristine markers of southward underthrusting that sequentially contributed to the growth of the duplex within the forearc crust. The subsequent exhumation of the metamorphic nappe stack was primarily driven by a major top-to-the-N detachment and a subordinate top-to-the-S detachment, which accommodated N-S-directed crustal extension. This extension later intermittently rotated to a E-W direction, as evidenced by the top-to-the-W detachment, reported here for the first time. This protracted extensional stress regime, active from the Miocene to the present, is responsible for the current geometry of the duplex, which is characterized by a regional-scale dome-like structure dissected by late normal faults. Subsidiary compressional and/or transpressional events perturbed this extensional deformation pattern, with a possible short-term recurrence linked to the megathrust seismic cycle. The finite structure of the H*P*-L*T* nappe-stack in western Crete, as revealed in this first contribution, lays the foundations for further petrological and geochronological investigations, presented in the companion paper (*Menant et al.*, 2026, this issue), to unravel the dynamics of deep accretion and exhumation that have shaped, and continue to shape, the evolution of the Hellenic forearc margin.

Acknowledgements

This work was funded by the A. von Humboldt foundation via a postdoctoral fellowship. The field campaigns carried on during this study were authorized by the Hellenic Survey of Geology and Mineral Exploration (HSGME) via the delivery of the work permit No. 3691/13-8-20. Nicolai Klitscher is warmly thanked for making the thin sections, as is Konstantinsos Soukis for insightful discussion in the field. We also thank Laura Federico and Graeme Eagles for their editorial handling of the manuscript and Edoardo Sanità and one anonymous reviewer for their constructive comments.

Author contributions

AM: conceptualization of the study, project funding, field work, original draft writing. **RA**: providing guidance throughout the Raman spectrometry analyses. **EB**, **LJ**: field work. **SA**: conceptualization of the study, field work. **OO**: conceptualization of the study. All the authors contributed to data analysis, as well as the review and editing of the original draft.

Data availability

The list of samples analyzed by RSCM thermometry with GPS coordinates and elevation and the complete RSCM dataset are provided in Supporting Information.

Competing interests

The authors declare no competing interests.

Peer review

This publication was peer-reviewed by Edoardo Sanità and an anonymous reviewer. The full peer-review report can be found here: Review Report.

Copyright notice

References

Agard, P., P. Monié, L. Jolivet, and B. Goffé (2002), Exhumation of the Schistes Lustrés complex: in situ laser probe $^{40}Ar/^{39}Ar$ constraints and implications for the Western Alps, *Journal of Metamorphic Geology*, *20*(6), 599–618, https://doi.org/10.1046/j.1525-1314.2002.00391.x.

Agard, P., A. Plunder, S. Angiboust, G. Bonnet, and J. Ruh (2018), The subduction plate interface: rock record and mechanical coupling (from long to short timescales), *Lithos*, *320-321*, 537–566, https://doi.org/10.1016/j.lithos.2018.09.029.

Allmendinger, R. W., N. Cardozo, and D. M. Fisher (2012), *Structural Geology Algorithms: Vectors & Tensor*, Cambridge University Press, Cambridge, England.

Angelier, J., N. Lybéris, X. Le Pichon, E. Barrier, and P. Huchon (1982), The tectonic development of the hellenic arc and the sea of crete: A synthesis, *Tectonophysics*, *86*(1-3), 159–196, https://doi.org/10.1016/0040-1951(82)90066-x.

Angiboust, S., J. Glodny, O. Oncken, and C. Chopin (2014), In search of transient subduction interfaces in the Dent Blanche–Sesia Tectonic System (W. Alps), *Lithos*, *205*, 298–321, https://doi.org/10.1016/j.lithos.2014.07.001.

Angiboust, S., J. Kirsch, O. Oncken, J. Glodny, P. Monié, and E. Rybacki (2015), Probing the transition between seismically coupled and decoupled segments along an ancient subduction interface, *Geochemistry, Geophysics,*

Geosystems: G(3), *16*(6), 1905–1922, https://doi.org/10.1002/2015gc005776.

Angiboust, S., A. Cambeses, T. Hyppolito, J. Glodny, P. Monié, M. Calderón, and C. Juliani (2018), A 100-m.y.-long window onto mass-flow processes in the Patagonian Mesozoic subduction zone (Diego de Almagro Island, Chile), *Geological Society of America Bulletin*, *130*(9-10), 1439–1456, https://doi.org/10.1130/b31891.1.

Angiboust, S., A. Menant, T. Gerya, and O. Oncken (2022), The rise and demise of deep accretionary wedges: A long-term field and numerical modeling perspective, *Geosphere*, *18*(1), 69–103, https://doi.org/10.1130/ges02392.1.

Aoya, M., Y. Kouketsu, S. Endo, H. Shimizu, T. Mizukami, D. Nakamura, and S. Wallis (2010), Extending the applicability of the Raman carbonaceous-material geothermometer using data from contact metamorphic rocks: RAMAN CARBONACEOUS-MATERIAL GEOTHERMOMETER, *Journal of Metamorphic Geology*, *28*(9), 895–914, https://doi.org/10.1111/j.1525-1314.2010.00896.x.

Armijo, R., H. Lyon-Caen, and D. Papanastassiou (1992), East-west extension and Holocene normal-fault scarps in the Hellenic arc, *Geology*, *20*(6), 491, https://doi.org/10.1130/0091-7613(1992)020<0491:eweahn>2.3.co;2.

Aubouin, J. (1959), Contribution à l'étude de la Grèce septentrionale; les confins de l'Epire et de la Thessalie, *Ann. Geol. Pays Hellen.*, *10*, 1–483.

Augier, R., G. Booth-Rea, P. Agard, J. M. Martínez-Martínez, L. Jolivet, and J. M. Azañón (2005), Exhumation constraints for the lower Nevado-Filabride Complex (Betic Cordillera, SE Spain): a Raman thermometry and Tweequ multiequilibrium thermobarometry approach, *Bulletin de la Societe Geologique de France*, *176*(5), 403–416, https://doi.org/10.2113/176.5.403.

Bachmann, R., O. Oncken, J. Glodny, W. Seifert, V. Georgieva, and M. Sudo (2009), Exposed plate interface in the European Alps reveals fabric styles and gradients related to an ancient seismogenic coupling zone, *Journal of Geophysical Research*, *114*(B5), https://doi.org/10.1029/2008jb005927.

Bangs, N. L., and S. C. Cande (1997), Episodic development of a convergent margin inferred from structures and processes along the southern Chile margin, *Tectonics*, *16*(3), 489–503, https://doi.org/10.1029/97tc00494.

Bassett, D., and A. B. Watts (2015), Gravity anomalies, crustal structure, and seismicity at subduction zones: 2. Interrelationships between fore-arc structure and seismogenic behavior: CRUSTAL STRUCTURE AND SEISMICITY: 2. FORE-ARC STRUCTURE, *Geochemistry, Geophysics, Geosystems: G(3)*, *16*(5), 1541–1576, https://doi.org/10.1002/2014gc005685.

Beaudoin, A., R. Augier, V. Laurent, L. Jolivet, A. Lahfid, V. Bosse, L. Arbaret, A. Rabillard, and A. Menant (2015), The Ikaria high-temperature Metamorphic Core Complex (Cyclades, Greece): Geometry, kinematics and thermal structure, *Journal of Geodynamics*, *92*, 18–41, https://doi.org/10.1016/j.jog.2015.09.004.

Behr, W. M., and R. Bürgmann (2021), What's down there? The structures, materials and environment of deep-seated slow slip and tremor, *Philosophical Transactions. Series A, Mathematical, Physical, and Engineering Sciences*, *379*(2193), 20200,218, https://doi.org/10.1098/rsta.2020.0218.

Beyssac, O., B. Goffé, C. Chopin, and J. N. Rouzaud (2002), Raman spectra of carbonaceous material in metasediments: a new geothermometer: RAMAN SPECTROSCOPY OF CARBONACEOUS MATERIAL, *Journal of Metamorphic Geology*, *20*(9), 859–871, https://doi.org/10.1046/j.1525-1314.2002.00408.x.

Beyssac, O., L. Bollinger, J.-P. Avouac, and B. Goffé (2004), Thermal metamorphism in the lesser Himalaya of Nepal determined from Raman spectroscopy of carbonaceous material, *Earth and Planetary Science Letters*, *225*(1-2), 233–241, https://doi.org/10.1016/j.epsl.2004.05.023.

Bonneau, M. (1984), Correlation of the Hellenide nappes in the south-east Aegean and their tectonic reconstruction, *Geological Society Special Publication*, *17*(1), 517–527, https://doi.org/10.1144/gsl.sp.1984.017.01.38.

Bonneau, M., and J. R. Kienast (1982), Subduction, collision et schistes bleus; l'exemple de l'Egee (Grece), *Bulletin de la Societe Geologique de France*, *S7-XXIV*(4), 785–791, https://doi.org/10.2113/gssgfbull.s7-xxiv.4.785.

Bouhot, M., A. Menant, C. Ganino, S. Angiboust, O. Oncken, L. Jolivet, D. Deldicque, N. Skarpelis, and F. Orange (2025), 3D Petro-structural evolution of the high pressure-low temperature Phyllite-Quartzite nappe pile in southern Peloponnese, Greece, *Tectonics*, *44*(12), e2025TC009,089, https://doi.org/10.1029/2025tc009089.

Burov, E., L. Jolivet, L. Le Pourhiet, and A. Poliakov (2001), A thermomechanical model of exhumation of high pressure (HP) and ultra-high pressure (UHP) metamorphic rocks in Alpine-type collision belts, *Tectonophysics*, *342*(1-2), 113–136, https://doi.org/10.1016/s0040-1951(01)00158-5.

Chatzaras, V., P. Xypolias, and T. Doutsos (2006), Exhumation of high-pressure rocks under continuous compression: a working hypothesis for the southern Hellenides (central Crete, Greece), *Geological Magazine*, *143*(6), 859–876, https://doi.org/10.1017/s0016756806002585.

Chatzaras, V., P. Xypolias, S. Kokkalas, and I. Koukouvelas (2013), Tectonic evolution of a crustal-scale oblique ramp, Hellenides thrust belt, Greece, *Journal of Structural Geology*, *57*, 16–37, https://doi.org/10.1016/j.jsg.2013.10.003.

Clift, P., and P. Vannucchi (2004), Controls on tectonic accretion versus erosion in subduction zones: Implications for the origin and recycling of the continental crust: SUBDUCTION TECTONICS, *Reviews of Geophysics (Washington, D.C.: 1985)*, *42*(2), https://doi.org/10.1029/2003rg000127.

Clift, P. D., and A. J. Hartley (2007), Slow rates of subduction erosion and coastal underplating along the Andean margin of Chile and Peru, *Geology*, *35*(6), 503, https://doi.org/10.1130/g23584a.1.

Cloos, M., and R. L. Shreve (1988), Subduction-channel model of prism accretion, melange formation, sediment subduction, and subduction erosion at convergent plate margins: 2. Implications and discussion, *Pure and Applied Geophysics*, *128*(3-4), 501–545, https://doi.org/10.1007/bf00874549.

Creutzburg, N., and E. Seidel (1975), zum stand der Geologie des präneagens auf Kreta, *N. Jb. Geol. Paläont. Abh.*, *149*(3), 363–383.

Dercourt, J., L. P. Zonenshain, L.-E. Ricou, V. G. Kazmin, X. Le Pichon, A. L. Knipper, C. Grandjacquet, I. M. Sbortshikov, J. Geyssant, C. Lepvrier, D. H. Pechersky, J. Boulin, J.-C. Sibuet, L. A. Savostin, O. Sorokhtin, M. Westphal, M. L. Bazhenov, J. P. Lauer, and B. Biju-Duval (1986), Geological evolution of the tethys belt from the atlantic to the pamirs since the LIAS, *Tectonophysics*, *123*(1-4), IN1–315, https://doi.org/10.1016/0040-1951(86)90199-x.

Dumitru, T. A., J. Wakabayashi, J. E. Wright, and J. L. Wooden (2010), Early Cretaceous transition from nonaccretionary behavior to strongly accretionary behavior within the Franciscan subduction complex: ACCRETION IN THE FRANCISCAN COMPLEX, *Tectonics*, *29*(5), https://doi.org/10.1029/2009tc002542.

Erdman, M. E., and C.-T. A. Lee (2014), Oceanic- and continental-type metamorphic terranes: Occurrence and exhumation mechanisms, *Earth-Science Reviews*, *139*, 33–46, https://doi.org/10.1016/j.earscirev.2014.08.012.

Fassoulas, C., A. Kilias, and D. Mountrakis (1994), Postnappe stacking extension and exhumation of high-pressure/low-temperature rocks in the island of Crete, Greece, *Tectonics*, *13*(1), 127–138, https://doi.org/10.1029/93tc01955.

Fassoulas, C., J. M. Rahl, J. Ague, and K. Henderson (2004), Patterns and conditions of deformation in the Plattenkalk nappe , Crete , Greece : A preliminary study, *Deltio tis Ellinikis Geologikis Etairias/Bulletin of the Geological Society of Greece*, *36*(4), 1626, https://doi.org/10.12681/bgsg.16566.

Gabalda, S., O. Beyssac, L. Jolivet, P. Agard, and C. Chopin (2009), Thermal structure of a fossil subduction wedge in the Western Alps, *Terra nova*, *21*(1), 28–34, https://doi.org/10.1111/j.1365-3121.2008.00849.x.

Gallen, S. F., K. W. Wegmann, D. R. Bohnenstiehl, F. J. Pazzaglia, M. T. Brandon, and C. Fassoulas (2014), Active simultaneous uplift and margin-normal extension in a forearc high, Crete, Greece, *Earth and Planetary Science Letters*, *398*, 11–24, https://doi.org/10.1016/j.epsl.2014.04.038.

Gautier, P., J.-P. Brun, and L. Jolivet (1993), Structure and kinematics of Upper Cenozoic extensional detachment on Naxos and Paros (Cyclades Islands, Greece), *Tectonics*, *12*(5), 1180–1194, https://doi.org/10.1029/93tc01131.

Gerya, T. V., B. Stöckhert, and A. L. Perchuk (2002), Exhumation of high-pressure metamorphic rocks in a subduction channel: A numerical simulation: EXHUMATION OF HIGH-PRESSURE ROCKS, *Tectonics*, *21*(6), 6–1–6–19, https://doi.org/10.1029/2002tc001406.

Glodny, J., and U. Ring (2022), The Cycladic Blueschist Unit of the Hellenic subduction orogen: Protracted high-pressure metamorphism, decompression and reimbrication of a diachronous nappe stack, *Earth-Science Reviews*, *224*(103883), 103,883, https://doi.org/10.1016/j.earscirev.2021.103883.

Grasemann, B., B. Huet, D. A. Schneider, A. H. N. Rice, N. Lemonnier, and C. Tschegg (2018), Miocene postorogenic extension of the Eocene synorogenic imbricated Hellenic subduction channel: New constraints from Milos (Cyclades, Greece), *Geological Society of America Bulletin*, *130*(1-2), 238–262, https://doi.org/10.1130/b31731.1.

Grasemann, B., D. A. Schneider, and A. Rogowitz (2019), Back to normal: Direct evidence of the Cretan Detachment as a north-directed normal fault during the Miocene, *Tectonics*, *38*(8), 3052–3069, https://doi.org/10.1029/2019tc005582.

Greiling, R. (1982), The metamorphic and structural evolution of the Phyllite-Quartzite Nappe of western Crete, *Journal of Structural Geology*, *4*(3), 291–297, https://doi.org/10.1016/0191-8141(82)90015-3.

Guillot, S., K. Hattori, P. Agard, S. Schwartz, and O. Vidal (2009), Exhumation processes in oceanic and continental subduction contexts: A review, in *Subduction Zone Geodynamics*, edited by J. P. Brun, O. Oncken, H. Weissert, C. Dullo, S. Lallemand, and F. Funiciello, Frontiers in Earth Sciences, pp. 175–205, Springer Berlin Heidelberg, Berlin, Heidelberg, https://doi.org/10.1007/978-3-540-87974-9_10.

Gutscher, M.-A., N. Kukowski, J. Malavieille, and S. Lallemand (1996), Cyclical behavior of thrust wedges: Insights from high basal friction sandbox experiments, *Geology*, *24*(2), 135, https://doi.org/10.1130/0091-7613(1996)024<0135:cbotwi>2.3.co;2.

Hoth, S., A. Hoffmann-Rothe, and N. Kukowski (2007), Frontal accretion: An internal clock for bivergent wedge deformation and surface uplift, *Journal of Geophysical Research*, *112*(B6), https://doi.org/10.1029/2006jb004357.

Jolivet, L. (2003), Subduction tectonics and exhumation of high-pressure metamorphic rocks in the Mediterranean orogens, *American Journal of Science*, *303*(5), 353–409, https://doi.org/10.2475/ajs.303.5.353.

Jolivet, L., and J.-P. Brun (2010), Cenozoic geodynamic evolution of the Aegean, *International Journal of Earth Sciences*, *99*(1), 109–138, https://doi.org/10.1007/s00531-008-0366-4.

Jolivet, L., J. M. Daniel, C. Truffert, and B. Goffé (1994), Exhumation of deep crustal metamorphic rocks and crustal extension in arc and back-arc regions, *Lithos*, *33*(1-3), 3–30, https://doi.org/10.1016/0024-4937(94)90051-5.

Jolivet, L., B. Goffé, P. Monié, C. Truffert-Luxey, M. Patriat, and M. Bonneau (1996), Miocene detachment in Crete and exhumation P-T-t paths of high-pressure metamorphic rocks, *Tectonics*, *15*(6), 1129–1153, https://doi.org/10.1029/96tc01417.

Jolivet, L., B. Goffé, R. Bousquet, R. Oberhänsli, and A. Michard (1998), Detachments in high-pressure mountain belts, Tethyan examples, *Earth and Planetary Science Letters*, *160*(1-2), 31–47, https://doi.org/10.1016/s0012-821x(98)00079-x.

Jolivet, L., F. Trotet, P. Monié, O. Vidal, B. Goffé, L. Labrousse, P. Agard, and B. Ghorbal (2010), Along-strike variations of P–T conditions in accretionary wedges and syn-orogenic extension, the HP–LT Phyllite–Quartzite Nappe in Crete and the Peloponnese, *Tectonophysics*, *480*(1-4), 133–148, https://doi.org/10.1016/j.tecto.2009.10.002.

Klein, T., J. P. Craddock, and G. Zulauf (2013), Constraints on the geodynamical evolution of Crete: insights from illite crystallinity, Raman spectroscopy and calcite twinning above and below the 'Cretan detachment', *International Journal of Earth Sciences*, *102*(1), 139–182, https://doi.org/10.1007/s00531-012-0781-4.

Kopp, H. (2013), Invited review paper: The control of subduction zone structural complexity and geometry on margin segmentation and seismicity, *Tectonophysics*, *589*, 1–16, https://doi.org/10.1016/j.tecto.2012.12.037.

Kotowski, A. J., M. Cisneros, W. M. Behr, D. F. Stockli, K. Soukis, J. D. Barnes, and D. Ortega-Arroyo (2022), Subduction, underplating, and return flow recorded in the cycladic blueschist unit exposed on syros, Greece, *Tectonics*, *41*(6), https://doi.org/10.1029/2020tc006528.

Kouketsu, Y., T. Mizukami, H. Mori, S. Endo, M. Aoya, H. Hara, D. Nakamura, and S. Wallis (2014), A new approach to develop the Raman carbonaceous material geothermometer for low-grade metamorphism using peak width: Raman CM geothermometer using FWHM, *Island Arc*, *23*(1), 33–50, https://doi.org/10.1111/iar.12057.

Krahl, J., G. Kauffmann, H. Kozur, D. Richter, O. Förster, and F. Heinritzi (1983), Neue Daten zur Biostratigraphie und zur tektonischen Lagerung der Phyllit-Gruppe und der Trypali-Gruppe auf der Insel Kreta (Griechenland), *Geologische Rundschau*, *72*(3), 1147–1166, https://doi.org/10.1007/bf01848358.

Lahfid, A., O. Beyssac, E. Deville, F. Negro, C. Chopin, and B. Goffé (2010), Evolution of the Raman spectrum of carbonaceous material in low-grade metasediments of the Glarus Alps (Switzerland): RSCM in low-grade metasediments, *Terra nova*, *22*(5), 354–360, https://doi.org/10.1111/j.1365-3121.2010.00956.x.

Lallemand, S. E., P. Schnürle, and J. Malavieille (1994), Coulomb theory applied to accretionary and nonaccretionary wedges: Possible causes for tectonic erosion and/or frontal accretion, *Journal of Geophysical Research*, *99*(B6), 12,033–12,055, https://doi.org/10.1029/94jb00124.

Laurent, V., L. Jolivet, V. Roche, R. Augier, S. Scaillet, and G. L. Cardello (2016), Strain localization in a fossilized subduction channel: Insights from the Cycladic Blueschist Unit (Syros, Greece), *Tectonophysics*, *672-673*, 150–169, https://doi.org/10.1016/j.tecto.2016.01.036.

Laurent, V., S. Scaillet, L. Jolivet, R. Augier, and V. Roche (2021), 40Ar behaviour and exhumation dynamics in a subduction channel from multi-scale 40Ar/39Ar systematics in phengite, *Geochimica et cosmochimica acta*, *311*, 141–173, https://doi.org/10.1016/j.gca.2021.06.001.

Lister, G. S., and G. A. Davis (1989), The origin of metamorphic core complexes and detachment faults formed during Tertiary continental extension in the northern Colorado River region, U.S.A, *Journal of Structural Geology*, *11*(1-2), 65–94, https://doi.org/10.1016/0191-8141(89)90036-9.

Lister, G. S., G. Banga, and A. Feenstra (1984), Metamorphic core complexes of Cordilleran type in the Cyclades, Aegean Sea, Greece, *Geology*, *12*(4), 221, https://doi.org/10.1130/0091-7613(1984)12<221:mccoct>2.0.co;2.

Lohrmann, J., N. Kukowski, C. M. Krawczyk, O. Oncken, C. Sick, M. Sobiesiak, and A. Rietbro (2006), Subduction channel evolution in brittle fore-arc wedges — a combined study with scaled sandbox experiments, seismological and reflection seismic data and geological field evidence, in *The Andes*, edited by O. Oncken, G. Chong, G. Franz, P. Giese, H.-J. Götze, V. A. Ramos, M. R. Strecker, and P. Wigger, pp. 237–262, Springer Berlin Heidelberg, https://doi.org/10.1007/978-3-540-48684-8_11.

Marrett, R., and R. W. Allmendinger (1990), Kinematic analysis of fault-slip data, *Journal of Structural Geology*, *12*(8), 973–986, https://doi.org/10.1016/0191-8141(90)90093-e.

Marsellos, A. E., W. S. F. Kidd, and J. I. Garver (2010), Extension and exhumation of the HP/LT rocks in the Hellenic forearc ridge, *American Journal of Science*, *310*(1), 1–36, https://doi.org/10.2475/01.2010.01.

Maruyama, S., J. G. Liou, and M. Terabayashi (1996), Blueschists and eclogites of the world and their exhumation, *International Geology Review*, *38*(6), 485–594, https://doi.org/10.1080/00206819709465347.

Menant, A., L. Jolivet, and B. Vrielynck (2016), Kinematic reconstructions and magmatic evolution illuminating crustal and mantle dynamics of the eastern Mediterranean region since the late Cretaceous, *Tectonophysics*, *675*, 103–140, https://doi.org/10.1016/j.tecto.2016.03.007.

Menant, A., S. Angiboust, and T. Gerya (2019), Stress-driven fluid flow controls long-term megathrust strength and deep accretionary dynamics, *Scientific Reports*, *9*(1), 9714, https://doi.org/10.1038/s41598-019-46191-y.

Menant, A., S. Angiboust, T. Gerya, R. Lacassin, M. Simoes, and R. Grandin (2020), Transient stripping of subducting slabs controls periodic forearc uplift, *Nature Communications*, *11*(1), 1823, https://doi.org/10.1038/s41467-020-15580-7.

Menant, A., J. Glodny, S. Angiboust, E. R. Sobel, E. Bessière, L. Jolivet, R. Augier, and O. Oncken (2026), Setting the Sequence of Slicing Events Along Deep Subduction Interfaces: 2. *P-T* Conditions and Timing of Accretion and Exhumation in Western Crete (Hellenic Margin), *Tektonika*, *4*(1), 88–113, https://doi.org/10.55575/tektonika2026.4.1.107.

Mouslopoulou, V., G. M. Bocchini, S. Cesca, V. Saltogianni, J. Bedford, G. Petersen, M. Gianniou, and O. Oncken (2020), Earthquake swarms, slow slip and fault interactions at the western-end of the Hellenic Subduction System

precede the M_w 6.9 Zakynthos Earthquake, Greece, *Geochemistry, Geophysics, Geosystems: G(3)*, *21*(12), https://doi.org/10.1029/2020gc009243.

Nicol, A., V. Mouslopoulou, J. Begg, and O. Oncken (2020), Displacement accumulation and sampling of paleoearthquakes on active normal faults of Crete in the Eastern Mediterranean, *Geochemistry, Geophysics, Geosystems: G(3)*, *21*(11), https://doi.org/10.1029/2020gc009265.

Noda, A. (2016), Forearc basins: Types, geometries, and relationships to subduction zone dynamics, *Geological Society of America Bulletin*, *128*(5-6), 879–895, https://doi.org/10.1130/b31345.1.

Oleskevich, D. A., R. D. Hyndman, and K. Wang (1999), The updip and downdip limits to great subduction earthquakes: Thermal and structural models of Cascadia, south Alaska, SW Japan, and Chile, *Journal of Geophysical Research*, *104*(B7), 14,965–14,991, https://doi.org/10.1029/1999jb900060.

Ott, R. F., S. F. Gallen, K. W. Wegmann, R. H. Biswas, F. Herman, and S. D. Willett (2019), Pleistocene terrace formation, Quaternary rock uplift rates and geodynamics of the Hellenic Subduction Zone revealed from dating of paleoshorelines on Crete, Greece, *Earth and Planetary Science Letters*, *525*(115757), 115,757, https://doi.org/10.1016/j.epsl.2019.115757.

Papanikolaou, D. (1997), The tectonostratigraphic terranes of the Hellenides, *Ann. Geol. Pays Hellen.*, *37*, 495–514.

Papanikolaou, D., and E. Vassilakis (2010), Thrust faults and extensional detachment faults in Cretan tectono-stratigraphy: Implications for Middle Miocene extension, *Tectonophysics*, *488*(1-4), 233–247, https://doi.org/10.1016/j.tecto.2009.06.024.

Pichon, X. L., and J. Angelier (1979), The hellenic arc and trench system: A key to the neotectonic evolution of the eastern mediterranean area, *Tectonophysics*, *60*(1-2), 1–42, https://doi.org/10.1016/0040-1951(79)90131-8.

Platt, J. P. (1986), Dynamics of orogenic wedges and the uplift of high-pressure metamorphic rocks, *Geological Society of America Bulletin*, *97*(9), 1037, https://doi.org/10.1130/0016-7606(1986)97<1037:doowat>2.0.co;2.

Polonia, A., L. Torelli, G. Brancolini, and M.-F. Loreto (2007), Tectonic accretion versus erosion along the southern Chile trench: Oblique subduction and margin segmentation: SUBDUCTION PROCESSES IN SOUTHERNMOST CHILE, *Tectonics*, *26*(3), https://doi.org/10.1029/2006tc001983.

Rahl, J., K. Anderson, M. Brandon, and C. Fassoulas (2005), Raman spectroscopic carbonaceous material thermometry of low-grade metamorphic rocks: Calibration and application to tectonic exhumation in Crete, Greece, *Earth and Planetary Science Letters*, *240*(2), 339–354, https://doi.org/10.1016/j.epsl.2005.09.055.

Ring, U., and F. Yngwe (2018), "to be, or not to be, that is the question"—the Cretan extensional detachment, Greece, *Tectonics*, *37*(9), 3069–3084, https://doi.org/10.1029/2018tc005179.

Ring, U., M. T. Brandon, S. D. Willett, and G. S. Lister (1999), Exhumation processes, *Geological Society Special Publication*, *154*(1), 1–27, https://doi.org/10.1144/gsl.sp.1999.154.01.01.

Ring, U., P. W. Layer, and T. Reischmann (2001), Miocene high-pressure metamorphism in the Cyclades and Crete, Aegean Sea, Greece: Evidence for large-magnitude displacement on the Cretan detachment, *Geology*, *29*(5), 395, https://doi.org/10.1130/0091-7613(2001)029<0395:mhpmit>2.0.co;2.

Ring, U., J. Glodny, T. Will, and S. Thomson (2010), The Hellenic subduction system: High-pressure metamorphism, exhumation, normal faulting, and large-scale extension, *Annual Review of Earth and Planetary Sciences*, *38*(1), 45–76, https://doi.org/10.1146/annurev.earth.050708.170910.

Ring, U., C. Fassoulas, I. T. Uysal, R. Bolhar, K. Tong, and A. Todd (2022), Nappe imbrication within the Phyllite-Quartzite Unit of west Crete: Implications for sustained high-pressure metamorphism in the hellenide subduction orogen, Greece, *Tectonics*, *41*(11), https://doi.org/10.1029/2022tc007430.

Roche, V., L. Jolivet, D. Papanikolaou, E. Bozkurt, A. Menant, and G. Rimmelé (2019), Slab fragmentation beneath the Aegean/Anatolia transition zone: Insights from the tectonic and metamorphic evolution of the Eastern Aegean region, *Tectonophysics*, *754*, 101–129, https://doi.org/10.1016/j.tecto.2019.01.016.

Romagny, A., L. Jolivet, A. Menant, E. Bessière, A. Maillard, A. Canva, C. Gorini, and R. Augier (2020), Detailed tectonic reconstructions of the Western Mediterranean region for the last 35 Ma, insights on driving mechanisms, *Bulletin de la Societe Geologique de France*, *191*, 37, https://doi.org/10.1051/bsgf/2020040.

Ruh, J. B. (2020), Numerical modeling of tectonic underplating in accretionary wedge systems, *Geosphere*, *16*(6), 1385–1407, https://doi.org/10.1130/ges02273.1.

Scholl, D. W. (2019), Seismic imaging evidence that forearc underplating built the accretionary rock record of coastal North and South America, *Geological Magazine*, *158*(1), 104–117, https://doi.org/10.1017/s0016756819000955.

Scholl, D. W., S. H. Kirby, R. von Huene, H. Ryan, R. E. Wells, and E. L. Geist (2015), Great (Mw8.0) megathrust earthquakes and the subduction of excess sediment and bathymetrically smooth seafloor, *Geosphere*, *11*(2), 236–265, https://doi.org/10.1130/ges01079.1.

Schwartz, S., P. Allemand, and S. Guillot (2001), Numerical model of the effect of serpentinites on the exhumation of eclogitic rocks: insights from the Monviso ophiolitic massif (Western Alps), *Tectonophysics*, *342*(1-2), 193–206, https://doi.org/10.1016/s0040-1951(01)00162-7.

Seidel, E., H. Kreuzer, and W. Harre (1982), A late Oligocene/early Miocene high pressure belt in the external Hellenides, *Geol. Jahrb. , Reihe E*, *23*, 165–206.

Seidel, M., E. Seidel, and B. Stöckhert (2007), Tectono-sedimentary evolution of lower to middle Miocene half-graben basins related to an extensional detachment fault (western Crete, Greece), *Terra nova*, *19*(1), 39–47,

https://doi.org/10.1111/j.1365-3121.2006.00707.x.

Shirzaei, M., R. Bürgmann, O. Oncken, T. R. Walter, P. Victor, and O. Ewiak (2012), Response of forearc crustal faults to the megathrust earthquake cycle: InSAR evidence from Mejillones Peninsula, Northern Chile, *Earth and Planetary Science Letters*, *333-334*, 157–164, https://doi.org/10.1016/j.epsl.2012.04.001.

Soujon, A., V. Jacobshagen, and E. Manutsoglu (1998), A lithostratigraphic correlation of the Plattenkalak occurences of Crete (Greece), *Deltio tis Ellinikis Geologikis Etairias/Bulletin of the Geological Society of Greece*, *32*(1), 41–48.

Stöckhert, B., M. Wachmann, M. Küster, and S. Bimmermann (1999), Low effective viscosity during high pressure metamorphism due to dissolution precipitation creep: the record of HP–LT metamorphic carbonates and siliciclastic rocks from Crete, *Tectonophysics*, *303*(1-4), 299–319, https://doi.org/10.1016/s0040-1951(98)00262-5.

Sutherland, R., V. Stagpoole, C. Uruski, C. Kennedy, D. Bassett, S. Henrys, M. Scherwath, H. Kopp, B. Field, S. Toulmin, D. Barker, S. Bannister, F. Davey, T. Stern, and E. R. Flueh (2009), Reactivation of tectonics, crustal underplating, and uplift after 60 Myr of passive subsidence, Raukumara Basin, Hikurangi-Kermadec fore arc, New Zealand: Implications for global growth and recycling of continents: RAUKUMARA BASIN, NZ, *Tectonics*, *28*(5), https://doi.org/10.1029/2008tc002356.

Theye, T., E. Seidel, and O. Vidal (1992), Carpholite, sudoite, and chloritoid in low-grade high-pressure metapelites from Crete and the Peloponnese, Greece, *European Journal of Mineralogy*, *4*(3), 487–508, https://doi.org/10.1127/ejm/4/3/0487.

Thomson, S. N., B. Stöckhert, and M. R. Brix (1998), Thermochronology of the high-pressure metamorphic rocks of Crete, Greece: Implications for the speed of tectonic processes, *Geology*, *26*(3), 259, https://doi.org/10.1130/0091-7613(1998)026<0259:tothpm>2.3.co;2.

Tortorici, L., R. Caputo, and C. Monaco (2010), Late Neogene to Quaternary contractional structures in Crete (Greece), *Tectonophysics*, *483*(3-4), 203–213, https://doi.org/10.1016/j.tecto.2009.05.020.

Uunk, B., F. Brouwer, M. de Paz-Álvarez, K. van Zuilen, R. Huybens, R. van 't Veer, and J. Wijbrans (2022), Consistent detachment of supracrustal rocks from a fixed subduction depth in the Cyclades, *Earth and Planetary Science Letters*, *584*(117479), 117,479, https://doi.org/10.1016/j.epsl.2022.117479.

van Hinsbergen, D. J. J., and J. E. Meulenkamp (2006), Neogene supradetachment basin development on Crete (Greece) during exhumation of the South Aegean core complex, *Basin research*, *18*(1), 103–124, https://doi.org/10.1111/j.1365-2117.2005.00282.x.

van Hinsbergen, D. J. J., E. Hafkenscheid, W. Spakman, J. E. Meulenkamp, and R. Wortel (2005a), Nappe stacking resulting from subduction of oceanic and continental lithosphere below Greece, *Geology*, *33*(4), 325, https://doi.org/10.1130/g20878.1.

van Hinsbergen, D. J. J., W. J. Zachariasse, M. J. R. Wortel, and J. E. Meulenkamp (2005b), Underthrusting and exhumation: A comparison between the External Hellenides and the "hot" Cycladic and "cold" South Aegean core complexes (Greece): UNDERTHRUSTING AND EXHUMATION IN GREECE, *Tectonics*, *24*(2), https://doi.org/10.1029/2004tc001692.

van Hinsbergen, D. J. J., T. H. Torsvik, S. M. Schmid, L. C. Maţenco, M. Maffione, R. L. M. Vissers, D. Gürer, and W. Spakman (2020), Orogenic architecture of the Mediterranean region and kinematic reconstruction of its tectonic evolution since the Triassic, *Gondwana Research: International Geoscience Journal*, *81*, 79–229, https://doi.org/10.1016/j.gr.2019.07.009.

Vidal, O., B. Goffé, and T. Theye (1992), Experimental study of the stability of sudoite and magnesiocarpholite and calculation of a new petrogenetic grid for the system FeO–MgO–Al_2O_3–SiO_2–H_2O, *Journal of Metamorphic Geology*, *10*(5), 603–614, https://doi.org/10.1111/j.1525-1314.1992.tb00109.x.

Vitale Brovarone, A., and D. Herwartz (2013), Timing of HP metamorphism in the Schistes Lustrés of Alpine Corsica: New Lu–Hf garnet and lawsonite ages, *Lithos*, *172-173*, 175–191, https://doi.org/10.1016/j.lithos.2013.03.009.

von Huene, R., and D. W. Scholl (1991), Observations at convergent margins concerning sediment subduction, subduction erosion, and the growth of continental crust, *Reviews of Geophysics*, *29*(3), 279–316, https://doi.org/10.1029/91rg00969.

Wang, K., and Y. Hu (2006), Accretionary prisms in subduction earthquake cycles: The theory of dynamic Coulomb wedge: DYNAMIC COULOMB WEDGE, *Journal of Geophysical Research*, *111*(B6), https://doi.org/10.1029/2005jb004094.

Wernado, G. (1983), Sedimentologische und fazielle untersuchungen in der Trypali-Einheit und in der Phyllit-Gruppe West- und Ostkretas, Ph.D. thesis, Universität München, Munich, Germany.

Wicker, V., and S. Bufféral (2024), Deformation mechanisms during the syn-orogenic extrusion of the high-Pressure Phyllites-Quartzites unit in the central and northern Peloponnese, Greece, *Tectonics*, *43*(8), https://doi.org/10.1029/2023tc008116.

Wijbrans, J. R., and I. McDougall (1986), 40Ar/39Ar dating of white micas from an Alpine high-pressure metamorphic belt on Naxos (Greece): the resetting of the argon isotopic system, *Contributions to mineralogy and petrology. Beitrage zur Mineralogie und Petrologie*, *93*(2), 187–194, https://doi.org/10.1007/bf00371320.

Wopenka, B., and J. Pasteris (1993), Structural characterization of kerogens to granulite-facies graphite; applicability of Raman microprobe spectroscopy, *The American Mineralogist*, *78*(5-6), 533–557.

Zachariasse, W. J., and D. van Hinsbergen (2025), Is there a Cretan supradetachment basin? Insights from detailed mapping on northwestern Crete (Greece), *Tektonika*, *3*(2), https://doi.org/10.55575/tektonika2025.3.2.97.

Zachariasse, W. J., D. J. J. van Hinsbergen, and A. R. Fortuin (2011), Formation and fragmentation of a late Miocene supradetachment basin in central Crete: implications for exhumation mechanisms of high-pressure rocks in the Aegean forearc: Formation and fragmentation of a late Miocene supradetachment basin, *Basin Research*, *23*(6), 678–701, https://doi.org/10.1111/j.1365-2117.2011.00507.x.

Zulauf, G., G. Kowalczyk, J. Krahl, R. Petschick, and S. Schwanz (2002), The tectonometamorphic evolution of high-pressure low-temperature metamorphic rocks of eastern Crete, Greece: constraints from microfabrics, strain, illite crystallinity and paleodifferential stress, *Journal of Structural Geology*, *24*(11), 1805–1828, https://doi.org/10.1016/s0191-8141(01)00168-7.

Zulauf, G., W. Dörr, L. Marko, and J. Krahl (2018), The late Eo-Cimmerian evolution of the external Hellenides: constraints from microfabrics and U–Pb detrital zircon ages of Upper Triassic (meta)sediments (Crete, Greece), *International Journal of Earth Sciences*, *107*(8), 2859–2894, https://doi.org/10.1007/s00531-018-1632-8.